IEEE Access
Multidisciplinary ⋮ Rapid Review ⋮ Open Access Journal

Received 27 November 2022, accepted 28 December 2022, date of publication 10 January 2023, date of current version 13 January 2023.

Digital Object Identifier 10.1109/ACCESS.2023.3235590

RESEARCH ARTICLE

Development of an Energy Management System for a Renewable Energy Community and Performance Analysis via Global Sensitivity Analysis

AMIR AHMADIFAR[1], (Member, IEEE), MIRKO GINOCCHI[1], MEGHA SHYAM GOLLA[1], FERDINANDA PONCI[1], (Senior Member, IEEE), AND ANTONELLO MONTI[1,2], (Senior Member, IEEE)

[1]E.ON Energy Research Center, Institute for Automation of Complex Power Systems, RWTH Aachen University, 52074 Aachen, Germany
[2]Fraunhofer-Institut für Angewandte Informationstechnik FIT, 52062 Aachen, Germany

Corresponding author: Amir Ahmadifar (amir.ahmadifar@eonerc.rwth-aachen.de)

This work was supported by the Platform for Operation of Distribution Networks (PLATONE), which is a European Project through the European Union's Horizon 2020 Research and Innovation Program, under Grant 864300.

ABSTRACT This paper presents the development of an energy management system (EMS) for a renewable energy community (REC) with the load-generation balancing objective. In this regard, rule-based and optimization mechanisms are proposed for the REC management in line with the scope of a field trial and considering the scarcity of the measurement and historical data. This typical data scarcity along with the intermittent behaviour of renewable energy resources introduce an unavoidable level of uncertainty— not being adequately addressed in the EMS literature— that might ultimately affect the proper REC management. Hence, a comprehensive performance analysis of the proposed EMS has been conducted via global sensitivity analysis (GSA). Particularly, variance-based sensitivity analysis has been employed to investigate how the variability of a set of selected indicators of the REC performance is apportioned to the different sources of uncertainty specifically related to the forecast and flexibility availability. Results show that the EMS performance is consistent with the EMS objective. The application of GSA reveals though interesting findings that contradict antecedent misconceptions about how different uncertainty sources affect the EMS performance. Although being related to the specific REC under study, the present work specializes GSA method in novel ways that pave the path for its reusability in the context of other EMS applications with different boundary conditions. By highlighting the necessity of GSA and showcasing its suitability to study the EMS performance under an uncertainty framework, the present work offers a precious tool to support system operators in their decision making process.

INDEX TERMS Battery energy storage system, energy management system, forecast, global sensitivity analysis, optimization, uncertainty analysis, variance-based sensitivity analysis.

I. INTRODUCTION

A. RENEWABLE ENERGY COMMUNITIES: OPERATION AND CHALLENGES

The conventional energy systems are experiencing a transition towards more decentralized and decarbonized solutions. On the path towards this changing paradigm, new business models and energy infrastructure ownership configurations are emerging [1]. In this regard, the concept of Renewable Energy Community (REC) is gaining increasing attention, both in literature and in the European Union (EU) regulatory framework which sets the path for the energy transition policies for 2030 and 2050. In particular, the latter defines RECs as legal entities with the primary purpose of proving

The associate editor coordinating the review of this manuscript and approving it for publication was F. R. Islam.

environmental, economic or social community benefits for its members, shareholders, or the local areas where they operate (EU Article 2(16) Recast Renewable Energy Directive). For the continuous provision of power supply within the future power grids, the RECs consisting of storage elements and Renewable Energy Sources (RES) could be exploited [2], [3], [4], [5]. For the optimal resource exploitation, the operation of an REC necessitates the implementation of an Energy Management System (EMS) in its control architecture [6]. In this regard, EMSs can support the reliable operation of the RECs and maximize the penetration of RES making use of forecasting information and the real-time monitoring of the grid together with the knowledge of operational constraints and the available storage and production capacities [7], [8]. Within an REC, many small-scale distributed energy resources generate energy surplus at the resource side which could be exchanged among different local consumers [9]. This energy exchange can potentially lead to the self-sufficiency and grid independence of the RECs which is referred to as the ''community self-consumption'' concept in the literature [10]. In the scope of an REC, a multi-perspective win-win situation can arise for both system operators and end customers with the help of energy management mechanisms and the controlled energy trading among different prosumers. From an environmental perspective, it expands the use of RES in power generation, resulting in lower greenhouse gas emissions. From a technical and economic viewpoint, local generation and consumption cut down power losses while postponing or eliminating the need of transmission and distribution infrastructure reinforcement. Furthermore, the self-consumption capability of RECs involves the use of different resources and helps diversifying centralized energy investments. From a socioeconomic viewpoint, distributed generation units within RECs expand the number of actors who are involved in the power generation chain, which were formerly concentrated in a small number of major corporations [11].

Apart from the benefits listed above, self-consuming RECs could potentially face some challenges. For instance, in the case of RECs with high Photovoltaic (PV) generation and low power demand, the generation excess might lead to the reverse power flow from the Low Voltage (LV) towards the Medium Voltage (MV) grid. According to studies [12], [13], a substantial volume of reverse power flow can affect the distribution feeder's voltage profile and increase distribution feeder voltages beyond the technical limits. In this regard, PV generation curtailment is a common solution in practice to avoid voltage violations. However, this leads to loss of energy generation possibly during the hours of a day with highest PV generation. Another solution would be the use of voltage regulation devices such as on-load tap changers and step voltage regulators. The main disadvantage associated with such devices is the significant increase in the mechanical stress and the consequent maintenance costs of such devices [14]. Alternatively, reactive power control mechanisms of the PV inverters could be another solution but the present utility practices (e.g., based on IEEE 1547 and UL 1741) pose a limit to this solution and only allow PVs to operate at a unity power factor [15], [16]. Additionally, the life time of PV inverters could be negatively impacted by such reactive power control mechanisms [17]. As an alternative to curtailment strategies, voltage regulation devices and reactive power control mechanisms, Battery Energy Storage System (BESS) units have proven to show potential in reducing the voltage rise issues in distribution networks with high shares of PV generation [18], [19]. In particular, BESS can store the excess of PV generation for either maximising self consumption or, in the case of need, injecting power back to the grid. This is the core concept behind the so-called ''virtual islanding'' mechanism which minimizes the power exchange through the MV/LV feeder and helps RECs become less dependant on the main power grid, ultimately reducing the burden on it. Furthermore, virtual islanding can save a considerable amount of renewable energy, shave the peak power exchanges on the MV/LV feeder, reduce power losses associated with power transportation along different feeders and ultimately improve the operation of the grid [20], [21]. This paper focuses on the EMS for the virtual islanding of an REC by resorting to a Distribution System Operator (DSO)-operated BESS. It is noteworthy that a virtually islanded REC is not intended to be totally isolated from the rest of the grid, as ''islanding'' refers here to the possibility of operating the REC without any additional power flow to and from the main grid.

B. RELATED WORK ON EMS DEVELOPMENTS

The majority of the existing EMS developments and the corresponding algorithms explicitly focus on the operation of community microgrids in grid-connected and islanding modes with different objective functions, such as BESS sizing, operational cost minimization, service restoration, power quality improvement, etc., and their corresponding operational and economical constraints, as extensively reviewed in [22], [23], [24], [25], [26], and [27]. There are also multiobjective EMS developments in literature within and outside the community microgrids context. Reference [28] for instance presents a combined optimization for the sizing of a hybrid energy storage system and an adaptive real-time EMS for electric vehicle applications.

In the literature, few works regarding EMS developments which are close to the context of the virtual islanding of the present paper can be found. For example, [29] presents a model for the optimal energy sharing in an energy community but with the objective function of minimizing the global energy cost rather than minimizing the energy exchange with the grid. Yet closer to the virtual islanding concept of the present work, [30] presents a microgrid multi-objective EMS for the minimization of energy exchange with the main grid while minimizing the operational cost and resistive power losses and maximizing the potential islanding time, though under the assumption of perfect load and generation forecasts. Moreover, [31] proposes an EMS in the context

of the management of REC energy storage systems for load-generation balancing schemes, although focusing on the minimization of energy from the grid specifically during high load peak conditions. In particular, the proposed EMS in [31] aims at peak load shaving and load shifting, considering PV forecast updates.

As similar attempts for load-generation EMS developments but specifically for the residential sector applications and not REC ones, PV self-consumption optimization has also been investigated in the literature, e.g., in [32]. In this area, some research work has also been dedicated to propose different rule-based self-consumption mechanisms, such as [33] that provides a rule-based strategy for the self-consumption maximization of the energy generated by a building integrated PV system through the usage of a household BESS unit.

C. UNCERTAINTY AND SENSITIVITY ANALYSIS IN EMS APPLICATIONS

The inherent unpredictability and randomness of RES and the stochastic behavior of consumers make their prediction and the consequent management systems of RECs challenging [34]. EMS developments dealing with controlling mechanisms in RECs must address one important aspect before reaching the readiness for applicable real-world settings, namely the uncertainty of different parameters of the EMS algorithms which may potentially affect them and impact the consequent decision making of the energy management problem. In this regard, underestimation and overestimation of the effect of EMS uncertain parameters can enforce additional unnecessary burden on possible revisions of the EMS algorithm. Therefore, the consideration of uncertainty sources for EMS applications is of critical importance.

In the context of balancing mechanisms of RECs, a number of research works have considered the intermittent behavior of renewable sources and loads. For instance, [35], [36], [37] provide some insights for the robust optimization of microgrids considering the uncertainty in renewable generation and/or load by means of data-driven approaches. However, although the volatility of RES and/or power load are considered into the implemented optimal management schemes, these studies do not perform a quantitative assessment of the contribution each uncertainty source(s) play in the performance of the supply-demand mechanisms of these microgrids. In [38] both weather and load uncertainties are taken into account for the optimal operation of RESs. However, the forecasting and optimization models are two separate parts and the exploration of the dynamic mechanism between these is not considered, with the focus being mainly towards the reduction of the forecast uncertainty rather than the interaction between these two above-mentioned parts. Similarly, [39] presents a management strategy for an EMS based on hourly forecast updating and a rescheduling mechanism. Although [39] tries to account for generation and load forecast errors, it does not consider the impact of each of them on the scheduling set-points and purely focuses on the reduction of the forecast error without considering the potential effect of the forecast uncertainty.

It is noteworthy that a crucial tool to properly quantify the impact of uncertainty sources on the EMS operation is represented by Sensitivity Analysis (SA). In relation to EMS—and, more broadly, to power systems—, SA is mainly conducted via ''perturb-and-observe'' approaches [40], whereby various uncertainty sources (referred to as ''inputs'') are changed with small perturbations and their effect on a specific quantity of interest (referred to as ''output'') is recorded. As discussed in Section III, these methods fall into the category of the so-called Local Sensitivity Analysis (LSA), according to which the impact of the uncertainty of the inputs on the output of interest is evaluated by varying one input at a time, while holding the others at their nominal values, hence studying the behavior of the system only around a specific baseline and neglecting the effect of possible interactions among inputs. As opposed to LSA, Global Sensitivity Analysis (GSA) encompasses a set of SA methods that accomplish an exploration of the whole variability of the inputs, without focusing on a given neighborhood around a specific baseline, hence revealing to be more effective to study the effects of large uncertainties and combinations thereof in complex power systems. To the best of authors' knowledge, no comprehensive SA studies have been performed for EMS algorithms under an uncertainty framework.

D. MOTIVATIONS AND CONTRIBUTIONS OF THE WORK

The present work aims at the EMS development for the virtual islanding of an REC, which can be considered as an essential step towards enhancing sustainability without affecting the whole system's efficiency and reliability and assuring the end user's comfort. Unlike the EMS developments reported in Subsection I-B (which do not directly address REC virtual islanding and/or neglect load/generation uncertainty), the balancing mechanism to be investigated in this work intends to manage an REC, despite the data scarcity and the uncertainty associated with it, to maximize the local energy consumption while minimizing the power exchange with the MV grid. In this work, the REC under study stems from the demonstration field trial investigated in the context of the EU Horizon 2020 Platone project [41], which is characterized by a high penetration level of distributed energy resources, is equipped with a BESS and has the major goal of undergoing virtual islanding despite the scarcity of measurement and historical data which naturally introduce a not negligible level of uncertainty.

As regards the analysis of EMS applications under an uncertainty framework, some attempts have been done in the literature to conduct SA to study the effect of the intermittent behavior of RES and assess their impact on the EMS operation, though mainly adopting LSA approaches. For instance, in [42], LSA is applied to a model predictive-based optimization model for a DC-coupled PV-storage system to investigate the performance of the system operation in response of

variations in the start time, duration and value of the time-of-use rate as well as fluctuations in the flat PV sell back price. Reference [43] presents an optimal scheduling model for a microgrid based on the temperature dependant thermal load modelling taking into account economical and technical constraints. Furthermore, a Monte Carlo based risk analysis is performed in order to rank the uncertainties in the thermal and electrical loads and outside temperature with respect to their impacts on the proposed model. On the other hand, GSA has been applied in very few cases in relationship with the EMSs. For instance, GSA is proposed in [44] to rank different inputs' uncertainties with respect to their impact on the loadability of an islanded microgrid. In particular, the objective function of this study is to maximise the system load margin, i.e., the distance between existing and critical operating points. However, unlike the current study in which the focus lies on the virtual islanding of an REC, [44] focuses on power flow calculations and the identification of the most influential inputs affecting the variability of selected outputs of interest, i.e., grid nodal powers and voltage magnitudes.

In light of the above discussion, the contributions of this paper are explained hereafter.

- An EMS with the supply-generation balancing objective is developed to enable the virtual islanding for the REC under study. The developed EMS, which consists of a balancer and a forecaster module, is capable of managing the REC in both measurement-and-steering and day-ahead scheduling modes by using the Rule-Based Balancing (RBB) and the Optimization (OPT) control mechanisms. In this regard and considering the limited data availability, the (near) real-time measurement and forecast values at the Point of Common Coupling (PCC) are used to enable the REC to experience the virtual islanding. The (near) real-time measurements are used as input of the measurement-and-steering mode to calculate the (near) real-time setpoints for steering the BESS based on the RBB mechanism in the form of a ''if (condition met), then (trigger the necessary action)''. The forecast values are used for calculating the day-ahead schedule of the BESS, using either RBB or OPT mechanisms. It should be stressed that the term (near) real-time in this work refers to the data communication or transfer using the state of the art communication protocols with small latency or delay for the whole system.
- A thorough analysis of the sensitivity behavior of the EMS algorithm for virtual islanding is conducted by GSA. To this aim, a set of outputs of interest is first carefully chosen, which encompass selected Key Performance Indicators (KPIs) to reflect different aspects concerning the EMS performance as well as relevant quantities for the REC operator within the scope of the virtual islanding scheme. Then, GSA is applied to investigate the impact of different sources of uncertainty (i.e., the variability of RES generation, loads and flexibility-related parameters) on the selected set of outputs of interest. In this regard, the benefits of the proposed multi-output GSA are manifold, as it (1) allows the identification of the combined effect of the influential model inputs with respect to the REC operator specific outputs, (2) helps in the potential reduction of the dimensionality (i.e., number of inputs) of the EMS algorithm (a feature which is especially useful for EMS models with a large number of uncertainty sources) and (3) guides in the consequent revision/refinement of the developed EMS model by focusing only on the influential inputs.
- The proposed multi-output GSA paves the path for its reusability in other EMS applications under an uncertainty framework. In fact, although the bindings of this research work with the field trial define the boundaries for the REC operating condition and the implemented EMS, the application of the proposed multi-output GSA is not restricted to the specific case study, but different replicates of the developed EMS (or, alternatively, different versions of it in other applications) might be similarly investigated, with proper modifications (if required) regarding the inputs/outputs to consider for the given application at hand.

E. STRUCTURE OF THE PAPER

This paper is organized as follows: Section II describes the structure of the EMS implemented in this work and describes the modelling of two EMS modules, i.e. the forecaster and the balancer; Section III describes the adopted workflow to perform GSA and provides mathematical details about the specific GSA method employed in this work (i.e., variance-based SA); Section IV elaborates on how GSA is applied specifically to study the performance of the two EMS modules; Sections V and VI present the results of the simulations and the performance analysis via GSA carried out on the balancer and the forecaster modules, respectively; Section VII concludes the paper.

II. DESCRIPTION OF THE DEVELOPED EMS

The EMS developed in this work has the objective of balancing generation and consumption within the REC under study. Fig. 1 shows the interactions among different actors of the developed EMS including the two modules, i.e., the forecaster and the balancer. With respect to the forecaster, the REC operator (in particular, the DSO in this specific field trial) with the help of a weather data provider and the Standard Load profile (SLP) is capable to forecast the aggregated consumption (P_{Ftc}) and generation (P_{Ftg}) profiles of the REC, respectively. In Subsection II-B, the forecasting mechanism of the net active power exchange at the PCC is better detailed. On the other hand, the balancer module is responsible for minimizing the power exchange at the PCC. The forecast (P_{Ftei}) or measurement ($P_{tei,meas}$) values of the active power exchange at the PCC are provided to the balancer, along with flexibility-related parameters, i.e., the flexibility capacity, minimum, maximum, and initial values of the State of Flexibility (SoF), and the maximum charging

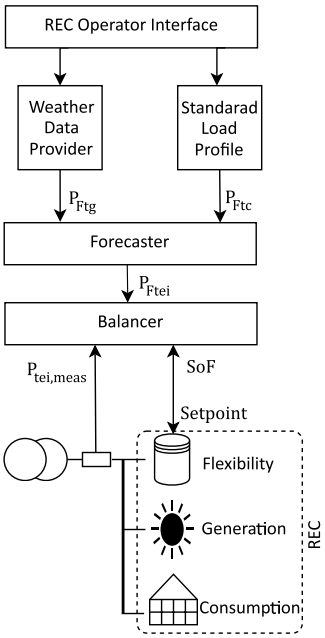

FIGURE 1. Schematic representation of the EMS.

and discharging power limits. In return, the balancer provides the day-ahead schedule (day-ahead setpoints) or the (near) real-time setpoint for the utilization of the flexibility during the forecast and measurement time windows, respectively. It should be stressed that ''flexibility capacity'' is intended as the total amount of available flexibility, minimum and maximum SoF represent the percentage-wise thresholds for using it, and the initial SoF represents the initial condition for steering it.

In short, the proposed EMS can monitor and steer the flexibility in a (near) real-time manner or provide a day-ahead schedule for steering it. The operation modes of the EMS can be categorized as:

- measurement-and-steering mode: steering of the flexibility according to (near) real-time setpoints calculated based on the (near) real-time measurements of the net active power at the PCC of the LV REC with the MV grid;
- scheduling mode: steering of the flexibility according to a day-ahead schedule calculated based on the forecast values of the net active power exchange at PCC.

For the (near) real-time steering of the flexibility, an RBB control logic is implemented making use of the available flexibility and (near) real-time measurements. As mentioned in Subsection I-D, the data exchange in this mode is done in a (near) real-time manner in compliance with the existing state of the art communication protocols. For providing the day-ahead schedules, both the RBB and OPT control mechanisms could be implemented. In Subsection II-C, these control mechanisms are elaborated in more detail.

A. ASSUMPTIONS AND OPERATIONAL CONDITIONS

- For the REC management and with respect to the availability of the forecast data, 24-h was selected as the reference length of the forecast and measurement time windows and the corresponding input profiles required respectively for the scheduling and measurement-and-steering modes. This is in line with the interest of the REC operator and the routine pattern of residential power load which corresponds to 24-h. In addition, the PV power generation forecast is available for the REC operator only as a day-ahead profile and without any updates during the 24-h forecast time window.
- For both the measurement-and-steering and scheduling modes, steering of the flexibility is done based on respectively the quarter-hourly (near) real-time measurement and forecast values leading to 96 setpoints for a day ($T = 96$).
- Based on the LV REC lines and ratings, the active power losses are neglected. Furthermore and considering the scarcity of measurement and forecast data, a single node approach is applied for the aggregation of renewable generation and load consumption within the REC under study [41].
- The main source of flexibility in the field trial and in the REC under study is a DSO-operated BESS. Other flexibility sources such as privately-owned storage units, heat pumps, etc. are out of the scope of the current study and will be investigated in future studies. Under the premise that all of the REC's renewable generating units are PV systems (with a total installed capacity of 300 kWp), this study focuses on the EMS function that offers day-ahead scheduling for the community BESS unit [41]. To keep the generality of the mathematical modelling though, the terminology ''Flexibility'' is used during the rest of this paper with a total capacity of $Flex_{cap} = 777$ kWh. It is noteworthy that the field trial focuses on the feasibility of the storage coordination for energy communities, whereas regulatory and business aspects thereof are not considered.
- Based on the field testings, no grid code deviations such as violations of nodal voltage and power line thermal constraints were observed by steering the BESS with the maximum charging and discharging powers.
- The focus of this virtual islanding study is the demand-generation balance and the minimization of active power exchange at the PCC for the REC. Voltage regulation, cost minimization, profit maximization, and other operational and economical objective functions are out of the scope of this study. Furthermore, the governance structure of the RECs and regulatory constraints associated with it are not the focus of the field trial and hence not considered in this paper.

B. FORECASTER

For the REC under study, the REC operator uses SLPs [45], as commonly done by energy suppliers when a recorded power measurement does not exist for electrical users. These SLPs replace the non-existent load profile curve of end customers with a reasonably precise estimate of energy

consumption with a quarter of an hour time resolution. They are representative load profiles for different end customer categories (residential, agricultural, and commercial), each of which may be considered to have comparable consumption patterns. With respect to the total generation of the RES, day-ahead generation profiles are delivered to the forecast module. A contractual agreement between the weather data provider and the REC operator is arranged to forecast the PV production of PVs installed within the REC [46].

Neglecting the power line losses, the net active power exchange at the PCC for each quarter-hourly time instance t, with $t \in \{00{:}00, 00{:}15, 00{:}30, \ldots, 23{:}45\}$, could be calculated as:

$$P^t_{Ftei} = P^t_{Ftc} - P^t_{Ftg} \tag{1}$$

where P^t_{Ftei}, P^t_{Ftc}, and P^t_{Ftg} refer to the forecast profiles of the net active power exchange at PCC, total consumption, and total generation, respectively, at the time instance t.

1) FORECAST CALIBRATION

As seen in (1), the forecast of the active power exchange at the PCC is calculated based on the total consumption (P_{Ftc}) and generation (P_{Ftg}) forecasts within the REC. Since the active power measurement data $P_{tei,meas}$ are available, the Root Mean Square Error (RMSE) of the forecast can be used as an indicator of the forecast accuracy and calculated as:

$$RMSE^d_{PFtei} = \sqrt{\frac{1}{T}\sum_{t=1}^{T}\left(P^t_{Ftei} - P^t_{tei,meas}\right)^2} \tag{2}$$

As net active power measurements at the PCC are available, the total generation and consumption forecast profiles are calibrated to improve the net power forecast profile. The calibration process starts with computing different forecast profiles for the total consumption and generation as:

$$\begin{cases} P^t_{F'tc} = m^d_{tc} P^t_{Ftc} + b^d_{tc} \\ P^t_{F'tg} = m^d_{tg} P^t_{Ftg} + b^d_{tg} \end{cases} \tag{3}$$

where d is the index representing the operation days in April (01.04.2021 till 27.04.2021 excluding 07, 17, 18, 23 and 24.04.2021). Furthermore, m^d_{tc}, b^d_{tc}, m^d_{tg}, and b^d_{tg} are the scaling factors used to create different generation and consumption forecast profiles ($P^t_{F'tc}$ and $P^t_{F'tg}$) varying in terms of magnitude and time. In absence of more detailed information about the reference profiles of generation and consumption, a uniform Probability Density Function (PDF) is chosen to characterize the uncertainty of the four scaling factors. The PDFs considered for the scaling factors are reported in Table 1, whereby the variation ranges of m_{tc}, b_{tc}, m_{tg}, and b_{tg} are selected based on plausible minimum and maximum values of the total generation and consumption profiles ($P^t_{F'tc}$ and $P^t_{F'tg}$). In particular, the installed capacity of the PV panels within REC as well as minimum and maximum measured values of $P_{tei,meas}$ during day and night hours are used to extract information regarding the trends of generation and consumption profiles and their corresponding peak values. Once the scaled profiles of $P^t_{F'tc}$ and $P^t_{F'tg}$ introduced in (3) are calculated, the scaled forecast of the net power at the PCC is calculated similar to (1). For the selection of the best scaled forecast of the net power profile, the one with the smallest RMSE is chosen. Such "best" scaled forecast profile is referred to as the calibrated forecast and denoted as ($P^d_{Ftei,new}$). Part 1 of the supplementary material provides an insight for the adopted forecast calibration scheme.

TABLE 1. Scaling factors and respective PDFs for the forecaster calibration.

Scaling factor	PDF
m^d_{tc}	$U[0.6, 1.5]$
m^d_{tg}	$U[0.7, 2]$
b^d_{tc}	$U[-5kW, 5kW]$
b^d_{tg}	$U[0kW, 10kW]$

C. BALANCER

In order to balance out the generation and consumption and minimize the active power exchange at the PCC, the balancer requires necessary information about the flexibility-related parameters. Furthermore, the net active power at the PCC is provided as input profile to the balancer for both measurement-and-steering and the day-ahead scheduling of the BESS. For the former case, in each instance of time, the balancer is provided with the active power measurement at the PCC, whereas for the latter case, the net active power forecast for the 24-hour scheduling horizon is provided to the balancer. In order to determine the setpoints for the measurement-and-steering mode, the RBB mechanism is applied, whereas for defining the day-ahead schedule, both the RBB and OPT mechanisms can be applied. Both balancing mechanisms are described hereafter.

1) OPT CONTROL MECHANISM

In order to minimize the exchange of power at the PCC for each instance of time t, both the import (P^t_{ti}) and the export (P^t_{te}) of power for the planning horizon (24 hours) should be minimized. This is mathematically formulated by the objective function in (4) together with the constraints in (5)–(11).

$$min \sum_{t=1}^{T}\left(P^t_{te} + P^t_{ti}\right) \tag{4}$$

subject to :

$$P^t_{te}, P^t_{ti}, P^t_{flex,dis}, P^t_{flex,ch} \geq 0 \tag{5}$$

$$P^t_{Ftg} + x^t_{dis}P^t_{flex,dis} + y^t_i P^t_{ti} = P^t_{Ftc} + x^t_{ch}P^t_{flex,ch} + y^t_e P^t_{te} \tag{6}$$

$$\begin{cases} 0 \leqslant x^t_{dis} + x^t_{ch} \leqslant 1 \quad \forall\{x^t_{dis}, x^t_{ch}\} \in \{0, 1\} \\ 0 \leqslant y^t_i + y^t_e \leqslant 1 \quad \forall\{y^t_i, y^t_e\} \in \{0, 1\} \end{cases} \tag{7}$$

$$SoF^{t+1} = SoF^t - x^t_{dis}\frac{P^t_{flex,dis}}{Flex_{cap}} + x^t_{ch}\frac{P^t_{flex,ch}}{Flex_{cap}}\Delta t \tag{8}$$

$$\begin{cases} 0 \leqslant P^t_{flex,dis} \leqslant P^{dis}_{flex,max} \\ 0 \leqslant P^t_{flex,ch} \leqslant P^{ch}_{flex,max} \end{cases} \tag{9}$$

$$min^d_{SoF} \leqslant SoF^t \leqslant max^d_{SoF} \tag{10}$$

$$SoF^{t=0} = initial^d_{SoF} \tag{11}$$

The constraint in (5) indicates that import and export powers as well as the charging ($P^t_{flex,ch}$) and discharging ($P^t_{flex,dis}$) powers are non-negative variables. The constraint in (6) assures the power balance between the generation and consumption: the left-side terms represent the total generation forecast (P^t_{Ftg}), discharging of the flexibility ($x^t_{dis}P^t_{flex,dis}$), total import ($y^t_i P^t_{ti}$) powers, while the right-side terms represent the total consumption forecast (P^t_{Ftc}), charging of the fleixbility ($x^t_{ch}P^t_{flex,ch}$), and total export ($y^t_e P^t_{te}$) powers from the REC. Additionally, the discrete variables of x^t_{dis}, x^t_{ch} and y^t_i, y^t_e ensure respectively that for each t, the simultaneous discharging/charging of the flexibility and import/export of power to/from the REC will not occur; this is formulated mathematically in (7). The flexibility-related constraints are formulated in (8)–(11). The dynamic representation for the state of flexibility in successive time intervals is reported in (8) where the variables SoF^t and SoF^{t+1} refer to the states of flexibility in two consecutive time instances considering the quarter hourly time difference of Δt. The parameters of maximum charging ($P^{ch}_{flex,max}$) and discharing ($P^{dis}_{flex,max}$) power limits in (9) define the power boundaries for the flexibility charging/discharging while the parameters of minimum (min^d_{SoF}) and maximum (max^d_{SoF}) allowable states of flexibility in (10) set the permissible range for the SoF^t. Finally, the initial state of flexibility at the beginning of the optimization time ($t = 0$) is dictated by the $initial^d_{SoF}$ paramater and represented in (11). It is noteworthy that the flexibility-related parameters of $initial^d_{SoF}$, min^d_{SoF}, and max^d_{SoF} are all reported in percentage of the total flexibility capacity $Flex_{cap}$; e.g., a 0% value of SoF shows full availability of the total capacity. Once all the flexibility-related parameters in addition to the forecast profiles are known for the optimization model, the optimal values of all the discrete and continuous variables are calculated based on the objective function (4).

In order to simplify the model and adapt it based on the inputs provided to the balancer, the import/export powers and the flexibility charging/discharging powers reported in (5)–(9) are substituted respectively by P^t_{tei} and P^t_{flex} in (12), with P^t_{tei} and P^t_{flex} being respectively the net active power exchange at the PCC and the flexibility setpoint for each t.

$$\begin{cases} P^t_{tei} = P^t_{ti} - P^t_{te} \\ P^t_{flex} = P^t_{flex,dis} - P^t_{flex,ch} \end{cases} \tag{12}$$

By using (1) and the variables introduced in (12), the mathematical description of the objective function (4) and the following constraints (5)–(9) can be reformulated as:

$$min \sum_{t=1}^{T} \left(P^t_{tei}\right)^2 \tag{13}$$

subject to the permissible range and initial constraints of state of flexibility reported in (10) and (11) and the following constraints:

$$P^t_{Ftei} = P^t_{flex} + P^t_{tei} \tag{14}$$

$$-P^{ch}_{flex,max} \leqslant P^t_{flex} \leqslant P^{dis}_{flex,max} \tag{15}$$

$$SoF^{t+1} = SoF^t - \frac{P^t_{flex}}{Flex_{cap}}\Delta t \tag{16}$$

In particular, the power balance constraint for the REC is stated in (14), whereas the power boundary constraint for the maximum charging and discharging powers and the dynamic representation of the state of flexibility are formulated in (15) and (16), respectively. Knowing the flexibility-related parameters and the forecast profile (P^t_{Ftei}), the optimal values of P^t_{tei}, P^t_{flex}, and SoF^t variables of the OPT mechanism are calculated based on the objective function (13).

2) RBB CONTROL MECHANSIM

The rule-based mechanism, following the ''if (condition met), then (trigger the necessary action)'' logic, balances out the overall consumption and generation within the REC while trying to avoid any power exchange in terms of import and export of power to and from the REC. As the positive and negative values of net active power at PCC (P^t_{tei}) in (12) indicate respectively a surplus and deficit of power within the REC, the discharging and charging mechanisms of the flexibility can be triggered according to (17) to avoid the import and export of power to and out of the REC:

$$P^t_{flex} + P^t_{tei} = 0 \tag{17}$$

Unlike the OPT mechanism, the P^t_{tei} in (17) is not a variable and is a priori known for triggering the steering of flexibility. Basically, the charging and discharging mechanisms of RBB are purely based on the known value of P^t_{tei} at each instance of time t and the available amount of flexibility. In other words, the flexibility is charged or discharged irrespective of future forecast and measurement values. Obviously, to ensure that the flexibility limitations are taken into consideration, the (dis)charging power constraint in (15), the dynamic representation of the state of flexibility constraint in (16) and the permissible range constraint for the state of flexibility in (10) remain valid for the RBB mechanism. In this regard and according to (17), the P^t_{flex} is calculated as the opposite sign of P^t_{tei} as long as the corresponding calculated state of flexibility based on (16) remains in the permissible range reported in (10). In other words, depending on the known value of P^t_{tei}, the flexibility is charged or discharged even extensively in case of high absolute values of P^t_{tei} till the power boundaries in (15) or SoF boundaries in (16) are reached and the flexibility is fully charged or discharged.

With respect to the application of RBB control mechanism for the operation modes of the developed EMS, the RBB control mechanism is the steering logic behind the measurement-and-steering mode of the EMS. For this operation mode, the $P^t_{tei,meas}$ measurement values are first provided to the balancer

(substituting the P^t_{tei} in (17)). Afterwards, according to the RBB control logic (17) and the constraints (10),(15), and (16), the flexibility is steered in a (near) real-time manner by setting the P^t_{flex} setpoints following the RBB logic to minimize the power exchange at the MV/LV feeder. On the other hand, the RBB control logic can also be applied for the day-ahead scheduling mode of the EMS apart from the OPT control mechanism described in Subsection II-C1. In this regard, instead of the P^t_{tei} in (17), the day-ahead forecast profile of P^t_{Ftei} is first provided to the balancer; then, by following the RBB control logic, the flexibility setpoints are calculated in the form of a day-ahead schedule.

III. SENSITIVITY ANALYSIS

In this work, GSA is adopted to assess the impact of different sources of uncertainty on the performance of the developed EMS. In this section some insights are provided regarding the general GSA methodology together with details of the mathematical formulation of variance-based SA, which is applied in this study.

A. PRELIMINARY DEFINITIONS

SA can be defined as *"the study of how uncertainty in the output of a model (numerical or otherwise) can be apportioned to different sources of uncertainty in the model input"* [47]. In particular the *inputs* are the model elements of interest (e.g., model equation parameters, initial and boundary conditions, time series, etc.) which are affected by some uncertainty due e.g. to inherent randomness, incorrect/partial knowledge, etc. The set of all possible combinations of the inputs' values is called *input space*. The *output* is the model response of concern obtained by running the model at any specific input value combination. Various techniques are available in the literature to perform SA and are mainly classified into local and global SA approaches [40]. In LSA methods (e.g., derivative-based techniques) the inputs' uncertainty is taken into account around a given baseline (e.g., the operational/nominal/optimal point) whereas GSA methods (mostly based on Monte Carlo simulations) aim at studying the full range of inputs' variability hence exploring the whole input space. It is noteworthy that LSA methods might turn out to be inefficient to fully investigate the overall effect of the model inputs' uncertainties if the model at hand features a certain degree of nonlinearities (e.g., interactive effects among inputs) and the inputs are affected by finite (also potentially large) uncertainty. To effectively address these circumstances GSA is commonly the suggested choice.

B. METHODOLOGY OF GLOBAL SENSITIVITY ANALYSIS

In this study, the general methodology for running GSA is adopted whose different steps are briefly summarized hereafter for the sake of convenience. For more details, the reader is referred to [40].

- The purpose of the analysis is defined beforehand.
- The simulation model to adopt is selected.
- The model output(s) of interest is (are) considered according to the analysis goals.
- The model inputs, which might have potential influence on the selected output, are identified. The model elements which, though entering the model definition, are not subject to SA, remain fixed at their nominal values.
- The uncertainty of the selected model inputs are characterized, e.g., in terms of PDF describing the analyst's degree of knowledge about the inputs' variability.
- The proper SA method to adopt for answering the analysis purpose is selected according to considerations such as computational cost to run the model, prior knowledge of the model, PDF type of the inputs, presence of correlation among inputs, etc.
- The N-dimensional input sample of the Monte Carlo simulation is generated by drawing from the input space a set of N values for each input according to specific sampling strategies (e.g., random or quasi-random numbers, etc.)
- The model response is collected by evaluating the model at the values of inputs' combinations specified by the input sample of the Monte Carlo simulation.
- The uncertainty analysis can be carried out by characterizing the output uncertainty via specific metrics of interest, such as mean, variance, confidence intervals, percentiles etc.
- The sensitivity indices of the selected SA method are extracted to understand the "origins" of the model output uncertainty. The whole analysis might be further iterated, e.g., to refine the inputs' uncertainty, to consider different inputs, etc.
- Graphical tools are utilized to provide an effective visualization of the results (e.g., via heatmaps, pie charts etc.) as well as to complement the information derived from the performed SA (e.g., via scatter plots, contour plots, coordinate plots, etc.)

C. VARIANCE-BASED SENSITIVITY ANALYSIS: MATHEMATICAL AND CONCEPTUAL FRAMEWORK

In this work, out of the different available GSA methods, the choice is made to adopt variance-based SA. Variance-based SA methods are widely considered as the "gold standard" to effectively study the effect of inputs' uncertainty, not only for their capability to flexibly deal with nonlinearities and large inputs' uncertainties but also for their model-free property, i.e., their ability to be applied in a trustworthy manner without requiring prior knowledge/information about the model properties (e.g., in the case of black-box models).

Consider a generic model $Y = g(X_1, X_2, \ldots, X_K)$, whereby Y is the model output (scalar for convenience) and $X_1, X_2, \ldots, X_K$ are the K model inputs, which are assumed to be independent random variables whose uncertainty is accounted for by specific PDFs. Variance-based SA aims at decomposing the total output variance Var(Y)

into contributions of individual inputs and combinations thereof [48]:

$$\mathrm{Var}(Y) = \sum_i \mathrm{Var}_i + \sum_i \sum_{i<j} \mathrm{Var}_{ij} + \ldots + \mathrm{Var}_{ij\ldots K} \quad (18)$$

where

$$\mathrm{Var}_i = \mathrm{Var}_{X_i}(\mathbb{E}_{\boldsymbol{X}_{\sim i}}(Y|X_i)) \quad (19)$$

$$\mathrm{Var}_{ij} = \mathrm{Var}_{X_{ij}}(\mathbb{E}_{\boldsymbol{X}_{\sim ij}}(Y|X_i, X_j)) + - \mathrm{Var}_{X_i}(\mathbb{E}_{\boldsymbol{X}_{\sim i}}(Y|X_i)) - \mathrm{Var}_{X_j}(\mathbb{E}_{\boldsymbol{X}_{\sim j}}(Y|X_j)) \quad (20)$$

and so on for higher order terms.

In particular the inner operator of (19), i.e., $\mathbb{E}_{\boldsymbol{X}_{\sim i}}(Y|X_i)$, is the expected value $\mathbb{E}$ of Y taken over $\boldsymbol{X}_{\sim i}$, i.e., all possible values of the inputs except X_i which is kept fixed, whereas the outside operator Var is the variance taken over all possible values of X_i. Accordingly, the term $\mathrm{Var}_{X_i}(\mathbb{E}_{\boldsymbol{X}_{\sim i}}(Y|X_i))$ describes the expected reduction of output variance that would be obtained if X_i could be fixed at its "true" (albeit unknown) value. Intuitively, if $\mathrm{Var}_{X_i}(\mathbb{E}_{\boldsymbol{X}_{\sim i}}(Y|X_i))$ is high, X_i is an important input in influencing $\mathrm{Var}(Y)$. As such, the quantity $\mathrm{Var}_{X_i}(\mathbb{E}_{\boldsymbol{X}_{\sim i}}(Y|X_i))$ may assume values ranging from 0 (when fixing X_i at its "true" value does not cause any output variance reduction) to $\mathrm{Var}(Y)$ (when fixing X_i at its "true" value fully determines the output variance $\mathrm{Var}(Y)$). This is due to the law of total variance:

$$\mathbb{E}_{X_i}(\mathrm{Var}_{\boldsymbol{X}_{\sim i}}(Y|X_i)) + \mathrm{Var}_{X_i}(\mathbb{E}_{\boldsymbol{X}_{\sim i}}(Y|X_i)) = \mathrm{Var}(Y) \quad (21)$$

where the term $\mathbb{E}_{X_i}(\mathrm{Var}_{\boldsymbol{X}_{\sim i}}(Y|X_i))$ can be interpreted as the residual output variance that would be achieved if X_i were fixed at its "true" value: $\mathbb{E}_{X_i}(\mathrm{Var}_{\boldsymbol{X}_{\sim i}}(Y|X_i))$ would be hence small if X_i is influential.

By normalizing $\mathrm{Var}_{X_i}(\mathbb{E}_{\boldsymbol{X}_{\sim i}}(Y|X_i))$ by the total output variance $\mathrm{Var}(Y)$, the so-called *first order Sobol' index* of input X_i is obtained:

$$S_i = \frac{\mathrm{Var}_{X_i}(\mathbb{E}_{\boldsymbol{X}_{\sim i}}(Y|X_i))}{\mathrm{Var}(Y)} \qquad S_i \in [0, 1] \quad (22)$$

whereby S_i assumes the meaning of the fraction of model output variance $\mathrm{Var}(Y)$ due to X_i *alone*, i.e., the individual contribution ("at the first order") of X_i to the total output uncertainty.

Similarly, the term Var_{ij} of (20) accounts for the variance contribution to $\mathrm{Var}(Y)$ due to the interactive effect of the inputs X_i and X_j, hence encapsulating the portion of model response which cannot be written simply as a superposition of the separate effects due to X_i and X_j. Intuitively, $\mathrm{Var}_{ij} \neq 0$ if $\mathrm{Var}_{X_{ij}}(\mathbb{E}_{\boldsymbol{X}_{\sim ij}}(Y|X_i, X_j)) \neq \mathrm{Var}_{X_i}(\mathbb{E}_{\boldsymbol{X}_{\sim i}}(Y|X_i)) + \mathrm{Var}_{X_j}(\mathbb{E}_{\boldsymbol{X}_{\sim j}}(Y|X_j))$. By normalizing Var_{ij} by the total output variance $\mathrm{Var}(Y)$, the so-called *second order Sobol' index* is obtained:

$$S_{ij} = \frac{\mathrm{Var}_{ij}}{\mathrm{Var}(Y)} \quad (23)$$

whereby S_{ij} assumes the meaning of the fraction of model output variance $\mathrm{Var}(Y)$ due to the combined effect between X_i and X_j after removing their first order effects S_i and S_j. Similar formulas hold for higher order indices up to the K-th interaction order.

By normalizing (18) by the total output variance $\mathrm{Var}(Y)$, the following relationship can be obtained:

$$\sum_i S_i + \sum_i \sum_{i<j} S_{ij} + \cdots + S_{ij\ldots K} = 1 \quad (24)$$

If the model is additive, i.e., it does not contain interactive effects among inputs, all terms of (24) higher than the first order are null and $\sum_i^K S_i = 1$. If interactions are present, the quantity $1 - \sum_i^K S_i$ is an indicator of the overall amount of interactions among inputs.

Equation (24) can be seen as a normalized decomposition of the total output variance with as many as $2K - 1$ terms. However, in practice, to avoid calculating all higher order terms, the so-called *total Sobol' index* for input X_i is instead computed [49]:

$$T_i = \frac{\mathbb{E}_{\boldsymbol{X}_{\sim i}}(\mathrm{Var}_{X_i}(Y|\boldsymbol{X}_{\sim i}))}{\mathrm{Var}(Y)} = 1 - \frac{\mathrm{Var}_{\boldsymbol{X}_{\sim i}}(\mathbb{E}_{X_i}(Y|\boldsymbol{X}_{\sim i}))}{\mathrm{Var}(Y)} \quad (25)$$

where $\mathrm{Var}_{\boldsymbol{X}_{\sim i}}(\mathbb{E}_{X_i}(Y|\boldsymbol{X}_{\sim i}))$ represents the variance reduction that would be obtained, on average, if all inputs except X_i could be fixed at their "true" values. On the other hand, the residual output variance $\mathbb{E}_{\boldsymbol{X}_{\sim i}}(\mathrm{Var}_{X_i}(Y|\boldsymbol{X}_{\sim i}))$ represents the contribution to the output variance due to all terms of any order—in the decomposition formula of (24)—that include X_i. Therefore, T_i accounts for the overall contribution of input X_i, including not only its first-order effect, but also all the other (higher-order) effects due to possible interactions with other inputs. For example, for a model with $K = 3$ inputs, the total Sobol' index for input X_i reads $T_1 = S_1 + S_{12} + S_{13} + S_{123}$. In general, $\sum_i^K T_i \geq 1$. Furthermore, $T_i - S_i$ signalizes how much the input X_i is involved in interactions with other model inputs: a high difference indicates that X_i owns an important interactive role in the model.

Sampling-based strategies exist for estimating Sobol' indices based on Monte Carlo simulation, i.e., starting from a set of finite combinations of input values and the corresponding model responses. To generate the input sample, various strategies may be employed and common practice is using "quasi-random" numbers [50], often preferred for their space-filling properties and enhanced numerical convergence rates (hence being particularly suitable for the numerical estimation of Sobol' indices [51]).

It is worth mentioning that the set of all the S_is together with all the T_is supplies the analyst with a comprehensive "big picture" of the model sensitivity pattern; higher-order Sobol' indices may be selectively computed only if specific model properties (such as interactions among specific couples of inputs) should undergo further investigation. As regards the computational cost, the full set of first order and total Sobol' indices can be obtained with $N(K + 2)$ model evaluations (with N usually varying between a few hundreds to one thousand), although alternative techniques are available to reduce the computational cost.

The two sensitivity measures S_i and T_i allow to answer specific research questions or analysis purposes [40], [47]. In particular, S_i provides the answer to the question: "What output variance reduction would be expected if uncertainty in X_i is removed?". Intuitively, the model inputs most contributing to the output uncertainty are those deserving more "attention", e.g., by collecting more "dedicated" measurements or additional information to decrease their uncertainty and ultimately reducing the model output variability. On the other hand, T_i supplies the answer to the question: "Which model inputs could be fixed anywhere in their variation range without affecting the output variance?". In other words, T_i allows detecting non-influential inputs that do not have significant importance on the output uncertainty (neither alone nor in synergy with other inputs). It can be proven that a necessary and sufficient condition for an input to be non-influential is $T_i \approx 0$: an almost null value of T_i hence signalizes that input X_i is inconsequential and can be fixed at any convenient value within their variation range (without appreciably losing information) and possibly eliminated from later analyses or to simplify the model structure.

IV. SENSITIVITY ANALYSIS FOR THE DEVELOPED EMS

In order to analyze the impact of the different uncertainty sources on the performance of the EMS, the GSA methodology summarized in Subsection III-B is adopted. Specifically, the inputs and outputs chosen for the two modules of the EMS, i.e., the balancer and the forecaster, are described hereafter.

A. SENSITIVITY ANALYSIS OF THE BALANCER

1) DEFINITION OF THE OUTPUTS OF THE BALANCER

In order to quantify the performance of the balancer with respect to its specific objective function, different KPIs are defined as SA outputs of interest, whose uncertainty is investigated with a multi-output SA. The selected KPIs are mathematically formulated in (26)–(30) and represent the relative improvement (in percentage terms) accomplished by implementing the balancing mechanism (subscript w) described in Subsection II-C with respect to the case without it (subscript wo). In particular, $RMSE^d_{bal}$ measures the relative improvement of the RMSE of the active power exchange at the PCC for day d with respect to its desired value $P_{tei,ref}$. On the other hand, MAX^d_{Pte}, MAX^d_{Pti}, AVG^d_{Pte} and AVG^d_{Pti} measure the relative improvement in, respectively, the maximum exported, maximum imported, average exported, and average imported active power to and from the REC.

$$RMSE^d_{bal} = \left(1 - \frac{RMSE^d_{Ptei,w}}{RMSE^d_{Ptei,wo}}\right) \times 100 \tag{26}$$

$$MAX^d_{Pte} = \left(1 - \frac{P^{d,t}_{te,max,w}}{P^{d,t}_{te,max,wo}}\right) \times 100 \tag{27}$$

$$MAX^d_{Pti} = \left(1 - \frac{P^{d,t}_{ti,min,w}}{P^{d,t}_{ti,min,wo}}\right) \times 100 \tag{28}$$

$$AVG^d_{Pte} = \left(1 - \frac{P^{d,t}_{te,avg,w}}{P^{d,t}_{te,avg,wo}}\right) \times 100 \tag{29}$$

$$AVG^d_{Pti} = \left(1 - \frac{P^{d,t}_{ti,avg,w}}{P^{d,t}_{ti,avg,wo}}\right) \times 100 \tag{30}$$

In (26), to capture the relative improvements in comparison to the baseline case without balancing mechanism, $RMSE^d_{Ptei,w}$ and $RMSE^d_{Ptei,wo}$ are defined as follows:

$$RMSE^d_{Ptei,w} = \sqrt{\frac{1}{T}\sum_{t=1}^{T}\left(P^t_{tei,w} - P_{tei,ref}\right)^2} \tag{31}$$

$$RMSE^d_{Ptei,wo} = \sqrt{\frac{1}{T}\sum_{t=1}^{T}\left(P^t_{tei,wo} - P_{tei,ref}\right)^2} \tag{32}$$

where $P^t_{tei,wo}$ and $P^t_{tei,w}$ refer to the net active power exchange at the PCC with and without the balancer, respectively, and could be calculated based on (33) and (34):

$$P^t_{tei,wo} = P^t_{tei,meas} \tag{33}$$

$$P^t_{tei,w} = P^t_{tei,meas} - P^t_{flex} \tag{34}$$

Similarly, for (27)–(30), the respective KPIs can be calculated using (33) and (34). In other words, for the calculation of the denominators in the second terms in the parentheses, (33) is used for calculating the maximum exported, maximum imported, average exported, and average imported active power to and from REC without the balancer mechanism. For the calculation of the numerators, (34) is used to account for the above-mentioned powers with the balancing mechanisms. For instance, the term $P^{d,t}_{ti,max,w}$ in (27) refers to the maximum imported power (P_{te} in kW) for day d at time instance t with (after) the use of the balancing mechanism and is calculated in the same manner as the maximum of the net power P_{tei} using (34). In short, (33) and (34) can be applied to net, import, and export powers.

It is noteworthy that the above-mentioned KPIs are in line with the virtual islanding mechanism and the corresponding operational conditions described in Subsection II-A and can provide the REC operator with unit-less indicators with respect to the baseline case (i.e., when the virtual islanding is not applied). The information derived from such KPIs can help the REC operator capture the different aspects associated with the MV/LV power exchange at the PCC for the REC under study in a comprehensive manner, i.e., investigating multiple aspects associated with the export, import and net powers at the PCC. In light of this, the target reference value for the net power exchange $P_{tei,ref}$ is purposefully highlighted in (31) and (32) in relation to typical contractual agreements, service requirements, and potential emerging grid codes for virtual islanding. For the REC under study in this research work, the target value is considered to be $P_{tei,ref} = 0$ kW.

Furthermore, should the REC operator be willing to use a total KPI for analyzing the overall performance of the balancer for a specific day d, a linear combination of the five different metrics listed in (26)–(30) can be built as:

$$\begin{aligned} total^{d}_{KPI} &= K_{rmse} \cdot RMSE^{d}_{bal} + K_{max,exp} \cdot MAX^{d}_{Pte} \\ &+ K_{max,imp} \cdot MAX^{d}_{Pti} + K_{avg,exp} \cdot AVG^{d}_{Pte} \\ &+ K_{avg,imp} \cdot AVG^{d}_{Pti} \end{aligned} \tag{35}$$

The weighting factors of each KPI in (35) are K_{rmse}, $K_{max,exp}$, $K_{max,exp}$, $K_{avg,exp}$, and $K_{avg,imp}$ and describe the interest of the REC operator for the performance of the balancer with respect to the $RMSE^{d}_{bal}$, MAX^{d}_{Pte}, MAX^{d}_{Pti}, AVG^{d}_{Pte}, and AVG^{d}_{Pti}, respectively. In order to keep the consistency with the previously defined KPIs, (36) is used to limit the maximum possible value of $total^{d}_{KPI}$ to 100%:

$$K_{rmse} + K_{max,exp} + K_{max,imp} + K_{avg,exp} + K_{avg,imp} = 1 \tag{36}$$

It is noteworthy that the values of the weighting factors and the corresponding total KPI are subject to the interest of the REC operator. In this study, $total^{d}_{KPI}$ is not the key indicator and therefore the different KPIs are weighted equally just to provide the REC operator with a single indicator if desired. In particular, positive values of the KPIs listed in (26)–(30) and (35) show improvements up to a maximum value of 100% indicating the best performance. On the other hand, negative values for these six KPIs signalize worsening of the performance after the implementation of the balancer with respect to the baseline case, i.e., no implementation of the balancer.

In addition to the above-mentioned five KPIs listed in (26)–(30), it might be of interest for the REC operator to investigate the uncertainty of the BESS final SoF ($final^{d}_{SoF}$) after the implementation of the balancing mechanism and realize what inputs mostly affect its variability. Therefore, $final^{d}_{SoF}$ is also considered as output of interest for the balancer SA.

2) SELECTION OF THE UNCERTAIN INPUTS OF THE BALANCER

As described in Section II, the performance of the balancer is potentially affected by the flexibility-related parameters such as the flexibility capacity, minimum and maximum SoF, initial SoF, maximum (dis)charging power capacities as well as P_{tei} profile which could inherently be affected by the intermittent weather and customer behaviors if the forecast profile is adopted for creating the day-ahead schedule. Hence, in this study, the inputs subject to SA—which, with their variability, may cause uncertainty in the expected results of the balancing mechanism with respect to the virtual islanding objective—are the initial $initial^{d}_{SoF}$, the minimum min^{d}_{SoF} and maximum max^{d}_{SoF} allowable SoFs (characterized by a continuous PDF), together with $fore_{sel}$ which is a discrete (integer-valued) input, assuming only three discrete values (i.e., 0, 1, 2) and acts as a "trigger" to select the forecast (P^{d}_{Ftei}), the calibrated forecast ($P^{d}_{Ftei,new}$), and the measurement ($P^{d}_{tei,meas}$) profiles, respectively. The inclusion of this discrete input allows for evaluating how sensitive the output is to the choice of utilizing the three different forecasts by simultaneously considering also the other three sources of uncertainty ($initial^{d}_{SoF}$, min^{d}_{SoF}, and max^{d}_{SoF}). The PDFs of the selected inputs and the outputs of interest for the balancer SA are reported in Table 2. On the other hand, other inputs such as the scheduling horizon (24 hour), the energy-wise amount of total flexibility capacity and the maximum (dis)charging power ratings are considered to be known without uncertainty (777 kWh and 300kW, respectively) and are not subject to SA. The results of conducting variance-based SA to investigate the balancer inputs' importance are reported in Subsection V-B.

B. SENSITIVITY ANALYSIS OF THE FORECASTER

1) DEFINITION OF THE OUTPUT OF THE FORECASTER

The forecast error reported in (2) is the indicator of the performance of the forecast module with respect to achieving an accurate net power exchange at the PCC. Therefore, for conducting SA on the forecaster module, $RMSE^{d}_{PFtei}$ is selected as output of the interest.

2) SELECTION OF THE UNCERTAIN INPUTS OF THE FORECASTER

As seen in (1), the forecast of the active power exchange at the PCC is calculated based on the total consumption (P_{Ftc}) and generation (P_{Ftg}) forecasts within the REC. As both types of forecast are affected by a certain amount of uncertainty related to their accuracy, it is first necessary to investigate their effect on the total power exchange forecast. To quantitatively analyse the impact of P_{Ftc} and P_{Ftg} on the $RMSE^{d}_{PFtei}$, a set of random profiles ($P^{t}_{F''_{tc}}$ and $P^{t}_{F''_{tg}}$) is produced according to (37) with the help of the scaling factors n_{tc} and n_{tg} characterized by the PDFs reported in column 2 of Table 3 (defined according to [52] and [53]). Afterwards, by subtracting $P^{t}_{F''_{tc}}$ from $P^{t}_{F''_{tg}}$, the corresponding sets of $P^{t}_{F''tei}$ profiles could be generated for which the output of interest reported in column 3 of Table 3 could be calculated

$$\begin{cases} P^{t}_{F''_{tc}} = n^{d}_{tc} P^{t}_{Ftc} \\ P^{t}_{F''_{tg}} = n^{d}_{tg} P^{t}_{Ftg} \end{cases} \tag{37}$$

The results of conducting variance-based SA to investigate the forecaster inputs' importance are reported in Subsection VI-B.

V. RESULTS FOR THE BALANCER

Knowing the EMS structure described in Section II and the operation boundaries associated with it (Section II-A), the simulation results for the developed balancer module of the EMS are reported hereafter. In particular, the results of the balancer module for the measurement-and-steering and scheduling modes are examined in Subsection V-A1 and Subsection V-A2, respectively. This is then followed by the complete SA analysis of the balancer performance with

TABLE 2. Summary of the selected model inputs and outputs for the balancer SA, with characterization of the inputs' uncertainty.

Input Name	Input PDF	Output 1	Output 2	Output 3	Output 4	Output 5	Output 6
$initial^d_{SoF}$ min^d_{SoF} max^d_{SoF} $fore_{sel}$	U[20, 85] U[5, 15] U[85, 95] U{0, 2}	$RMSE^d_{bal}$	MAX^d_{Pte}	MAX^d_{Pti}	AVG^d_{Pte}	AVG^d_{Pti}	$final^d_{SoF}$

TABLE 3. Summary of the selected model inputs and output for the forecaster SA, with characterization of the inputs' uncertainty.

Input Name	Input PDF	Output
n^d_{tc} n^d_{tg}	$N[1, 0.05]$ $N[1, 0.025]$	$RMSE^d_{PF''tei}$

respect to the uncertainty in the different inputs. The OPT optimization problem is solved with IPOPT [54] by interfacing it with Pyomo 5.7 [55] using a Lenovo ThinkPad T470s computer with Intel i7-7500 CPU, 2.90 GHz and 16 GB RAM. Furthermore and according to the data availability, the simulation results are represented for the selected operational days in April.

A. BALANCER PERFORMANCE

In this Section, the RBB and OPT mechanisms of the balancer are analyzed. First, in Subsection V-A1 the performance of the balancer is investigated when the measured profile is used as the input profile. In Subsection V-A2, the balancer's performance based on the provided forecast input data for creating the day-ahead schedule of the flexibility assets is examined considering the input profile of P^d_{Ftei} provided to the balancer module by the forecaster.

1) BALANCER PERFORMANCE WITH MEASURED INPUT PROFILE

In this Section, the performance of the balancer is investigated by using the measurement profile of $P_{tei,meas}$ for both RBB and OPT control mechanisms. Obviously, analyzing the performance of RBB logic with $P_{tei,meas}$ is an indicator of the EMS's performance for the measurement-and-steering mode.

Fig. 2 shows the performance of the RBB and OPT mechanisms for two selected days: on the left (04.04.2021), the total renewable generation is relatively low considering the total installed capacity of 300 kWp, whereas on the right (05.04.2021), the total renewable generation is relatively high. For the simulation results presented in this figure, the flexibility-related input parameters are fixed to the following values: $initial^d_{SoF} = 52.5\%$, $min^d_{SoF} = 5\%$, $max^d_{SoF} = 95\%$. As observed in Fig. 2, the RBB mechanism is able to minimise the active power exchange for a certain amount of time per day till the flexibility threshold in either min^d_{SoF} or max^d_{SoF} is reached. In other words and for the field trial case, the BESS is extensively discharged or charged till its boundaries are reached. After reaching these boundary conditions, the remaining power should be imported and exported, respectively. On the other hand, the OPT mechanism satisfactorily manages to minimize the active power exchange at the PCC considering the flexibility availability and its restrictions. Quantitatively, with respect to the performance indicators $RMSE^d_{bal}$, Max^d_{Pte}, Max^d_{Pti}, AVG^d_{Pte}, AVG^d_{Pti}, $total^d_{KPI}$, the OPT mechanism is able to respectively shave the peak export and import power profiles, reduce their average values, and overall reach the minimization objective for P_{tei} in a relatively better manner compared to RBB. On 04.04.2021 for instance, the above-mentioned KPIs have typically higher values for OPT than for RBB (i.e., 73.5%, 72.7%, 100%, 87.7%, 100% for OPT in comparison to 38.2%, 72.7%, 100%, 0%, 100%, 62.2% for RBB).

For different days under study, it is worth to mention that for OPT and with the measured input profile, no negative KPIs are recorded. However, for RBB, AVG^d_{pte} could assume negative values. The reason behind can be inferred by looking at the definition of this KPI in (29). For RBB and for certain days as observed in Part 2 of the supplementary material, the export of power is minimized for a certain amount of time till the peak generation hours arise. After reaching the threshold of the flexibility max^d_{SoF}, the remaining relatively high power production peaks should be exported and therefore leading to $P^{d,t}_{te,avg,w} > P^{d,t}_{te,avg,wo}$, hence yielding a negative AVG^d_{pte}.

As mentioned above, Fig. 2 shows the EMS's performance for a set of fixed flexibility-related inputs. To gain quantitative information regarding the variability of the different KPIs with respect to the input variations reported in Table 2 (apart from $fore_{sel}$ which is fixed at the specific value of 2 to represent the measured profile), Part 4.1 and 4.2 of the supplementary material depict the daily standard deviation and mean values of the listed outputs of interest, respectively. As observed for the case of using $P_{tei,meas}$ measurement values by the EMS, the typical daily mean values of $RMSE^d_{bal}$ are higher for OPT compared to RBB. As this output quantifies the performance of the balancer in reaching the zero power exchange at the PCC, higher mean values indicate better performance of OPT in comparison to RBB. Furthermore, the uncertainty in the $RMSE^d_{bal}$ values for OPT are typically lower than for RBB (comparing their ranges of variability and respective standard deviations). In other words, provided that there is no forecast error, OPT can achieve a better performance (higher mean value of $RMSE^d_{bal}$) with less uncertainty. On certain days, the export power with both RBB and OPT could be totally minimized to the zero reference value leading to the corresponding $AVG^d_{pte} = MAX^d_{pte} = 100\%$. For these days and without the forecast error, the peak generation is comparatively low, and considering the capacity of the storage unit, the surplus generation could be stored. On the other hand, for the days with high peak share of generation, the RBB approach is unable to avoid the export peaks as the threshold SoF_{max} will be reached before the peak generation hours. Therefore, for such days, $MAX^d_{pte} = 0\%$.

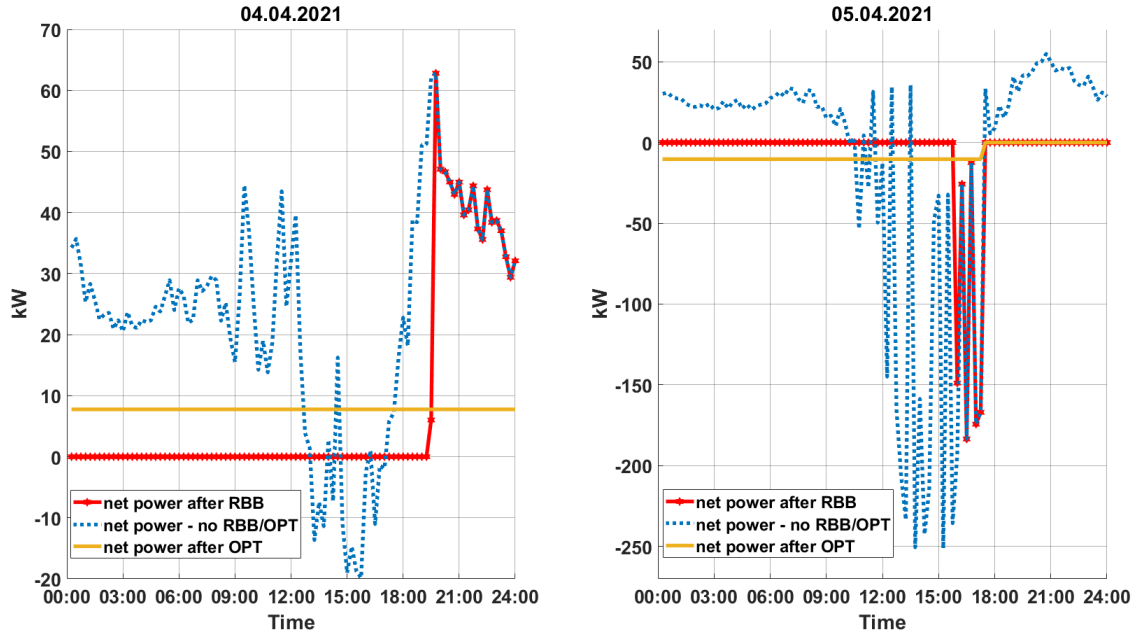

FIGURE 2. Balancer performance using the measured profile.

After analyzing the results associated with the performance of the balancer using only the measured profile, the following findings can be listed:

- The measurement-and-steering operation based on the RBB mechanism requiring the measured profile $P^d_{tei,meas}$ is able to accomplish the desired performance. However, on days with a considerably high amount of renewable generation with respect to the total installed capacity of 300kWp, the flexibility reaches its limit of max^d_{SoF} leading to the export of power from the REC. This problem exists inherently for RBB for the measurement-and-steering mode of operation and peak export powers cannot be avoided for an REC with relatively much higher total generation with respect to the total consumption. In this regard, investment decisions such as increasing the BESS capacity or operational decisions such as reducing the operational time under this mode could be of help for reducing peak export power.
- For the day-ahead scheduling, provided that there is no forecast error (i.e., zero uncertainty is assumed), OPT mechanism leads to an overall better performance which is reflected in the mean values of the different KPIs. Furthermore, in comparison to the RBB mechanism, there is no observation of negative KPIs, i.e., no undesired performance is expected.
- The introduction of different KPIs enables the REC operator to observe in detail the different aspects associated with the performance of the EMS. For instance, despite the fact that the overall performance of the OPT seems to be higher than that of RBB (when using the measured input profile), closer investigation of the average imported power at the PCC shows the slight superiority of RBB in this regard and for certain days.
- With respect to the uncertainty in the performance of the balancer module and in the absence of forecast uncertainty, OPT mechanism leads in general to lower variability of the outputs of interest. In this regard, using the different KPIs and/or outputs of interest enables the REC operator to investigate the uncertainty in a detailed manner.

2) BALANCER PERFORMANCE WITH UNCERTAIN INPUT PROFILE

In this Section, in addition to the uncertainty of flexibility-related input parameters of $initial^d_{SoF}$, min^d_{SoF}, and max^d_{SoF}, the uncertainty of the input profile used by the balancer module is also included into the analysis by considering $fore_{sel}$ as the fourth uncertain input which can assume the three integer values of 0, 1 and 2 representing, respectively, the selection of the forecast ($P^d_{Ftei} = 0$), calibrated forecast ($P^d_{Ftei,new} = 1$), and measured ($P^d_{tei,meas} = 2$) profiles. The combination of flexibility-related input parameters together with the type of input profile are provided to the balancer to calculate the setpoints based on the RBB and OPT mechanisms.

Fig. 3 provides an insight about the performance of the balancer for both OPT and RBB in presence of the forecast error and for two different days, with the flexibility-related input parameters set at $initial^d_{SoF} = 52.5\%$, $min^d_{SoF} = 5\%$, $max^d_{SoF} = 95\%$. On the left side, the calibrated forecast profile ($P^d_{Ftei,new}$) is used as input to the balancer for 04.04.2021 when the total renewable generation is relatively low considering the total installed capacity of 300 kWp. On the right side, the non-calibrated forecast profile P^d_{Ftei} is used as the input to the balancer for 05.04.2021 when the total renewable generation is relatively high. Considering the intermittent behavior of the renewable generation which is not

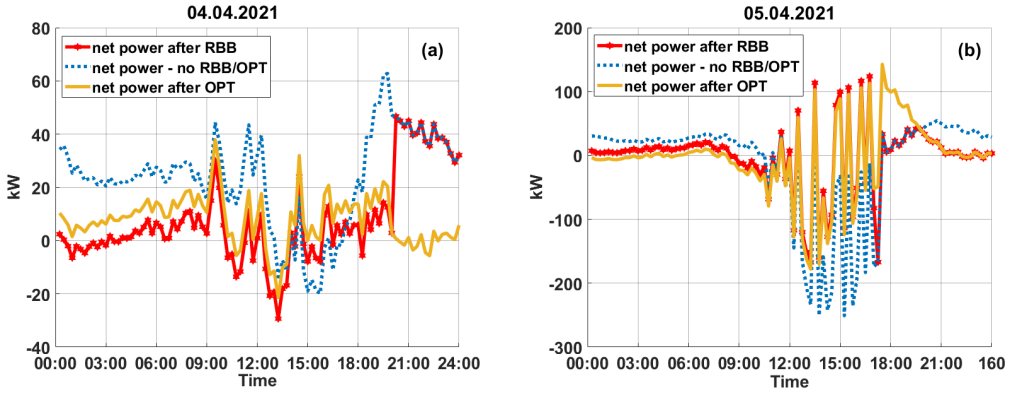

FIGURE 3. Balancer performance with (a) calibrated forecast and (b) forecast input profiles.

captured by the forecast profile, the difference between the forecast and measurement profiles can lead to import/export power profiles affecting the zero-power exchange objective. The flexibility setpoints P^t_{flex} are calculated according to the balancing objectives of OPT and RBB reported respectively in Subsections II-C1 and II-C2. Regardless of the forecast errors of different time steps t, the scheduled setpoints P^t_{flex} are calculated using the forecast value of $P^{d,t}_{Ftei}$ and based on the control actions associated with RBB and OPT mechanisms reported respectively in (17) and (13). Once the setpoints are defined, the corresponding $P^t_{tei,w}$ values after the implementation of these setpoints is also known according to (34). In particular, $P^t_{tei,w}$ values calculated based on the forecast profiles might lead to the unexpected/undesired power flow at the PCC ($|P^t_{tei,w}| > |P^t_{tei,wo}|$) corresponding to undesired export/import values according to (12). Part 3 of the supplementary material provides an insight about the forecast errors for an exemplary day with considerable amount of P_{tei} power fluctuations. Obviously, not being able to capture such fluctuations via the forecast affects the expected outcome of the balancer in the scheduling mode as the setpoints are calculated based on the values of the forecast input profile and not the measurement ones.

To have a detailed look at the daily evolution of the mean and standard deviations of the outputs considering the variability of $fore_{sel}$ (i.e., assuming uncertainty in the input profile), the reader can refer to Parts 4.1 and 4.2 of the supplementary material for RBB and OPT, respectively. For the majority of the days, not only the performance of the balancing mechanism is negatively impacted but also a significant increase in the variability of the different outputs of interest is observed. This is also summarized in Fig. 4 where the variability of mean and standard deviation values of the different outputs of interest over the different days is presented. For example, with respect to MAX^d_{Pti}, the magenta box plots of the mean values show a significant drop of the median value after the introduction of the forecast uncertainty, whereas a huge increase of the variability of the standard deviation and of its median can be also observed. To get an overall picture and for a complete comparison, the variability of mean and standard deviation of the same outputs when only the measured input profile is used by the balancer is also provided in Fig. 4 with the cyan box plots.

After analyzing the results associated with the performance of the balancer with uncertain input profile, the following findings can be listed:

- For the day-ahead scheduling, if forecast uncertainty is taken into account, OPT's performance is still in overall superior to that of RBB with respect to the mean values of the defined KPIs.
- Using the defined multiple KPIs enables the REC operator to fully investigate the performance of the OPT and RBB. In this regard, it was found out for instance that for both of these mechanisms, the maximum export power minimization is successful at the cost of increase in the peak of import power which is reflected in the negative values for the KPI associated with the peak power import at the PCC. This is due to the forecast uncertainty associated with the renewable generation and the corresponding intermittent behavior of renewable resources which is not captured by the forecast mechanism.
- With respect to the uncertainty in the performance of the balancer module and in the presence of forecast uncertainty, different outputs of interest show relatively large variability for both OPT and RBB. This finding contradicts the typical statements such as the ''obvious'' superiority of OPT over RBB, as the uncertainty in the desired performance looking at the different outputs of interest proves, for certain days, the opposite.

3) BALANCER PERFORMANCE AND NEGATIVE KPIs

According to (26)–(30) and (35), negative KPIs indicate worsening of the power exchange with respect to the deviation from the zero power exchange, maximum and average export and import powers, and the overall performance of the EMS. Fig. 5 summarizes the occurrence of negative KPIs for the combinations of different inputs for RBB and

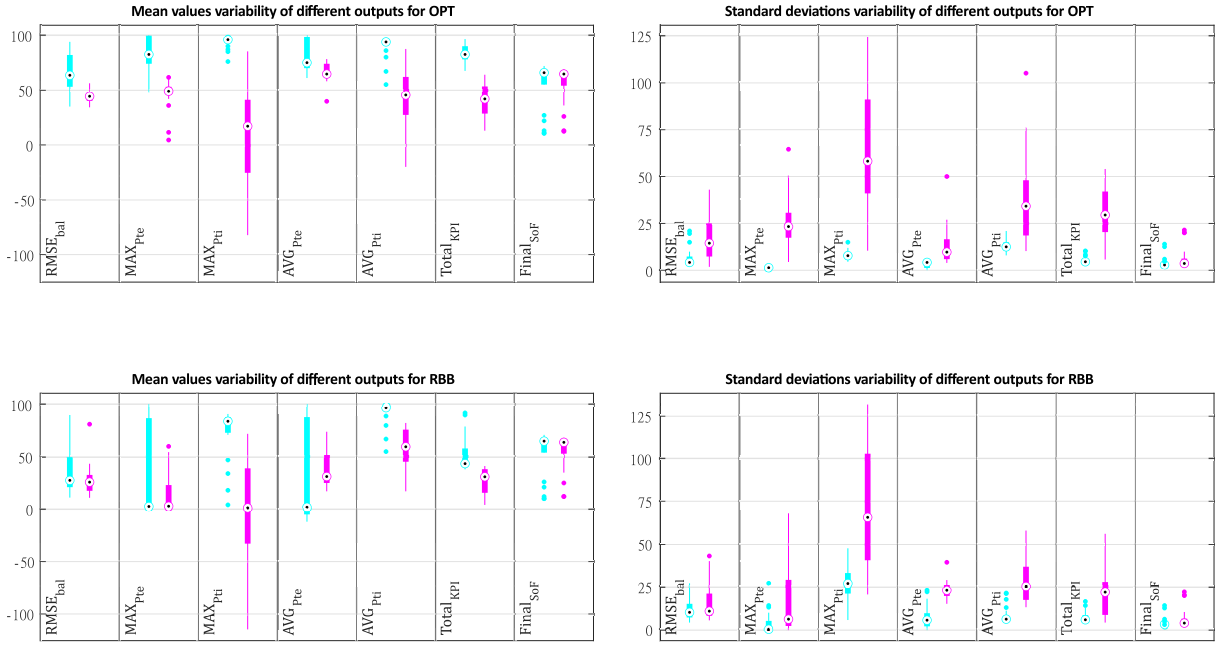

FIGURE 4. Variability of mean and standard deviation of different outputs over different days. Cyan box plots represent the case when only measurement profile is used, magenta box plots represent the case when forecast and measurement profiles are used.

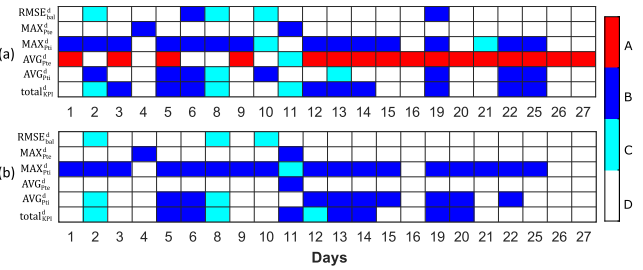

FIGURE 5. Occurrence of negative KPIs for (a) RBB and (b) OPT.A. With certain and uncertain input profile B. With uncertain input profile C. Occurrence can be avoided after forecast calibration D. No occurrence.

OPT. The obtained results in Subsection V-A1 showed that, without forecast uncertainty, no negative KPI is observed for OPT. On the other hand, for RBB and for certain days with relatively high shares of renewable generation for relatively long period of times, negative values of AVG^d_{Pte} can be observed even without the forecast uncertainty. This is due to the fact that the mean value of export power after the implementation of the balancing mechanism ($P^d_{te,avg,w}$) is calculated for shorter time periods and higher peak export values as observed in Fig. 2 for 05.04.2021. Red cells in Fig. 5 represent such days. This implies that, even if the (near) real-time steering mechanism is conducted for certain days, input combinations might worsen the average export power at the PCC after the balancing mechanism is implemented. By focusing only on $RMSE^d_{bal}$ as a proper indicator of the balancing mechanism performance, Fig. 5 shows that the forecast calibration can completely remove the occurrence of negative values for OPT. However, for RBB, even after forecast calibration, negative values of $RMSE^d_{bal}$ still occur in some days, e.g., on 06.04 and 19.04, as shown by the blue cells in the first row of Fig. 5a. For these specific days it would be of interest to investigate which input combinations led to negative values of $RMSE^d_{bal}$. To this scope, Fig. 6 shows the coordinate plots for 06.04 and 19.04: on the vertical axis, the range of variability of the inputs $initial^d_{SoF}$, min^d_{SoF}, and max^d_{SoF} are reported ($fore_{sel} = 1$, i.e., only the calibrated forecast input profile is used) and the combinations of the three inputs leading to negative values of $RMSE^d_{bal}$ are highlighted in red. From these plots it can be inferred that negative $RMSE^d_{bal}$ values are entirely due to high values of $initial^d_{SoF}$. In other words, $initial^d_{SoF}$ is the only responsible input for $RMSE^d_{bal}$ to be negative (irrespective of the values of min^d_{SoF}, and max^d_{SoF}): values of $initial^d_{SoF}$ higher than 70 % (for 06.04.2021) and higher than 60 % (for 19.04.2021) should be hence avoided assuring that the RBB mechanism starts with enough flexibility to account for the high renewable share during peak hours. The reader can refer to Part 5.1 of the supplementary material for a detailed look at the input combinations and the corresponding variations in the values of $RMSE^d_{bal}$.

Regarding MAX^d_{Pte}, after the forecast calibration on 04.04 and by avoiding high values of $initial^d_{SoF}$, negative values could be avoided for RBB and OPT as observed in Part 5.2 of the supplementary material. For 11.04 though, this would work only for RBB and not for OPT.

The situation for the peak import-related KPI, i.e., MAX^d_{Pti}, is challenged by the intermittent behavior of the renewables and the consequent fluctuations in the generation profiles. As the forecast profile (including the calibration) is not enough to capture such fluctuations, the peak values of import power after implementing the balancing mechanism ($P^d_{ti,max,w}$) are typically higher than the peak of the

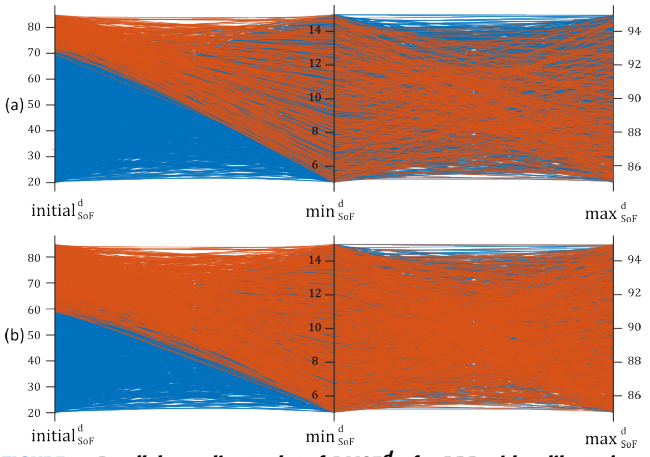

FIGURE 6. Parallel coordinate plot of $RMSE^{d}_{bal}$ for RBB with calibrated forecast input profile on (a) 06.04.2021 and (b) 19.04.2021.

original import profiles ($P^{d}_{ti,max,wo}$). Basically, peak shaving mechanism for the export power tries to minimise the high export forecast values. However, considering the above-mentioned fluctuations, the real measurement values turn out quite often to be smaller than the expected forecast ones in short time intervals (e,g., a power spike from 100 KW to 30 KW due to lower sun irradiation). As the schedule is calculated based on the forecast power profiles, lack of such high export values in reality should be compensated by importing power to the REC. Similarly, the average import power and consequently the AVG^{d}_{Pti} is negatively impacted by the above-mentioned intermittent behavior. To avoid negative values for both MAX^{d}_{Pti} and AVG^{d}_{Pti} KPIs, selecting proper ranges for $initial^{d}_{SoF}$ might help for certain days. This could be observed in Part 5.3 of the supplementary material: e.g., avoiding $initial^{d}_{SoF}$ higher than around 40% can prevent negative values of AVG^{d}_{Pti} for this day, too.

In short, after analyzing the occurrences of negative KPIs, it can be inferred that the improvement in the input forecast profile enhances the performance of OPT and RBB. For the former, simple methods such as the calibration can solely eliminate the occurrence of negative values for the output of interest describing the balancer's performance with respect to the zero target value for power exchange at the PCC. Furthermore and provided that sufficient data (e.g., additional meteorological data) are available, clusters of different operating days can be made for each KPIs. Knowing for which cluster which KPI experiences negative values, the REC operator can use the provided hints and combinations of flexibility-related input parameters (in presence of forecast uncertainty), and finally avoid the undesired negative performance with respect to that specific KPI for that specific cluster.

B. RESULTS OF THE BALANCER SENSITIVITY ANALYSIS

In Subsections V-A1 and V-A2, the variations of different outputs of interest considering different input combinations for both the measurement-and-steering and scheduling modes have been investigated, though selectively keeping fixed one or more of the balancer's uncertain inputs. In this Section, GSA is instead applied to explore the variability of all the balancer inputs according to the PDFs reported in Table 2. As a matter of fact, the application of GSA as a diagnostic tool can guide model calibration and verification, and support the prioritization of efforts for uncertainty reduction in a concrete and robust manner.

In light of this, GSA is been applied for RBB and OPT to assess, for different days, which is the sensitivity of the different outputs of interest with respect to the uncertainty of the considered inputs. The results are summarized in the heatmaps of Fig. 7 and Fig. 8 for RBB and OPT, respectively. These heatmaps visualize the total Sobol' indices, which provide the inputs' importance ranking taking into account the overall contribution of each input not only "per se" but also in interaction with other inputs. It can be observed from Fig. 7 and Fig. 8 that $fore_{sel}$ plays the biggest role in affecting most of the outputs of interest for both RBB and OPT. This shows the importance of focusing the efforts towards the reduction of forecast uncertainty by improving the forecast accuracy. On the other hand, GSA helps realizing why $fore_{sel}$ (and the consequent input profile variations) does not impact the variability of the standard deviations of certain outputs reported in Fig. 4. For example, in the case of $final^{d}_{SoF}$ and $RMSE^{d}_{bal}$, these variations were not considerably different from each other with and without the uncertain input profile (cyan versus magenta box plots, respectively). Investigating the total Sobol' index of $fore_{sel}$ reveals that the uncertainty of the input profile is either not influential or, in comparison to flexibility-related inputs, relatively less influential in the variations of the above-mentioned outputs.

Focusing on $RMSE^{d}_{bal}$ as the metric measuring the deviation of the balancing mechanism from the minimum power exchange at the PCC, it can be concluded from Fig. 7 that $RMSE^{d}_{bal}$ of RBB is quite sensitive against the variations in $initial^{d}_{SoF}$. This is due to the nature of the rule-based approach which strictly follows the forecast values at each time t and charges/discharges the BESS according to them. In such a case, the variations in the starting point, i.e. $initial^{d}_{SoF}$ can impact also significantly how the (dis)charging profile, i.e., the schedule, is going to be and therefore affect the variations in the $P^{d}_{tei,w}$ and $RMSE^{d}_{bal}$ reported in (34) and (26), respectively. On the other hand and by observing specifically the total Sobol' indices for $RMSE^{d}_{bal}$ in Fig. 8, the OPT mechanism shows relatively less sensitivity to the variations in $initial^{d}_{SoF}$ and this mechanism is able to plan the schedule in a more effective manner considering the whole optimization period and not purely based on forecast instances. Furthermore, by looking at the daily values of the total Sobol' indices for min^{d}_{SoF} and max^{d}_{SoF}, it can be observed that they do not show significant contribution to the uncertainty of KPIs introduced in (26)-(30). Therefore, these two inputs can be fixed anywhere in their variation range without affecting the balancer KPIs for RBB and OPT. As regards $final^{d}_{SoF}$, it can be said that min^{d}_{SoF} is typically non-influential for the developed RBB and OPT mechanisms. However, max^{d}_{SoF}

is quite an influential input for affecting the variability of $final^{d}_{SoF}$ for both RBB and OPT.

As mentioned in Subsection III-C, by computing the term $1-\sum S_i$, quantitative information regarding the total amount of model interactions can also be obtained. The level of interactions existing among the different balancer inputs is shown in Fig. 9 for RBB and OPT for the different days under study. As regards OPT, the amount of model interactions affecting is quite low for most of the days (values of $1-\sum S_i < 0.1$), whereas there are relatively higher interactions for RBB. For example, on 09.04 and 22.04, more than 30% of the variance of MAX^{d}_{Pte} is due to interactions among the different balancer inputs. To further investigate this contingency, the second order Sobol' indices S_{ij}s are computed specifically for these days: the values of the S_{ij}s show that the interactive effect among $initial_{SoF}$ and $fore_{sel}$ contributes to a worth 28% of the total variance of MAX^{d}_{Pe} ($S_{ij} = 0.28$ for the pair $\{initial_{SoF}, fore_{sel}\}$). This might be related to the patterns of the forecast profiles and how the initial condition at the beginning of the balancing mechanism can interact with it. In the case of $final^{d}_{SoF}$ and for both RBB and OPT, there are high interactions among $initial_{SoF}$ and $fore_{sel}$ with a second order Sobol' index of $S_{ij} = 0.42$, signalizing that the variations in the $final^{d}_{SoF}$ are greatly influenced by the joint effect of these two inputs.

Moreover, Fig. 8 shows that $initial^{d}_{SoF}$ is of importance for the variation of some KPIs on some days. As mentioned in Subsection V-A2, proper selection of $initial^{d}_{SoF}$ after the forecast calibration could be helpful in avoiding negative KPI occurrences for certain days. Typically, the range of final state of flexibility for the preceding day, i.e., $final^{d-1}_{SoF}$, is already in the "preferable" range of the initial state of flexibility for the upcoming day, i.e., $initial^{d}_{SoF}$ (where "preferable" range refers to the one avoiding negative KPIs). However, in some cases, fixing $final^{d-1}_{SoF}$ to a specific value might be of interest. For instance, in accordance to Part 5.3 of the supplementary material, to avoid negative values of AVG^{d}_{Pti}, low values of $initial^{d}_{SoF}$ are preferable. On the other hand, for the previous day, i.e., 13.04, $final^{d}_{SoF}$ is ranged between [62%, 74%]. Therefore, it might be of interest to set a fixed value of $final^{d}_{SoF}$ to have a fixed $initial^{d}_{final}$ for the upcoming day. This is only possible for the OPT by adding a constraint to the optimization problem and not for RBB as RBB mechanism basically follows strictly the forecast value at each time t to decide about the schedule setpoint(s) and the corresponding SoF value(s). Equation (38) shows this additional constraint for the OPT if fixing the final state of flexibility by the end of the optimization ($t = end$) to a predefined $final^{d}_{SoF}$ is of interest:

$$SoF^{t=end} = final^{d}_{SoF} \tag{38}$$

However, this advantage of OPT should be examined more carefully. The addition of the constraint in (38) to the optimization model changes both the model and the input space affecting the performance of the OPT mechanism. This additional constraint might have an important role in the variance of different outputs of interests. Therefore, SA should be conducted after revising the OPT mechanism (from here referred to as the revised OPT) with the outputs 1 to 5 defined in (26)–(30) and the inputs listed in Table 2, in addition to the newly introduced $final^{d}_{SoF}$ input with a uniform distribution $U[15\%, 85\%]$ covering the possible range for it. Fig. 11 shows the ranking for the revised OPT for the above-mentioned set of inputs and outputs. It can be concluded that for the majority of KPIs and for most of the days, $fore_{sel}$ is still the most influential input. Furthermore, it can be observed that $final^{d}_{SoF}$ plays an important role in the variation of the outputs of interest for the revised OPT. Interestingly, on 04.04 for instance, $initial^{d}_{SoF}$ and $final^{d}_{SoF}$ play an important role in the variations of $RMSE^{d}_{bal}$. With respect to the interactions, Fig. 12 shows that, in comparison to Fig. 9, more interactions can be observed among different inputs affecting the variance of different outputs. For instance, by looking at the second order Sobol' indices for AVG^{d}_{pti}, out of the 30% observed interactions, around half of it originates from the second order interactions among $fore_{sel}$ and $final_{SoF}$. Considering both the ranking and interactions, the revision of the OPT model (which in the first place was conducted to limit the occurrence of negative KPIs and improve the performance of OPT) leads to a more sensitive behavior with respect to the input variability. If the $final^{d}_{SoF}$ is not carefully selected, undesired values of different KPIs may occur as it was shown that the variability of this newly added model input, i.e., $final^{d}_{SoF}$, can have a significant impact on the variability of different outputs. Part 6 of the supplementary material shows the daily mean and standard deviations after the revision of OPT. It can be observed that for the majority of the days and most of the KPIs, introducing $final^{d}_{SoF}$ in the set of uncertain inputs leads to the slight reduction in the mean values and the slight increase in the standard deviations. This is in line with the results of GSA that highlights the importance of $final_{SoF}$ variations and their impact on the variations of different outputs.

According to the obtained results, the following findings could be listed with respect to the SA of the balancer.

- The application of GSA can fully support the ranking of influential parameters affecting the variability of outputs of interest. As an example, one could not observe that much of impact on the standard deviation variation of certain outputs of interest with and without the uncertain input profile in Fig. 4 (cyan vs magenta box plots, respectively). Once the total Sobol' indices are analyzed though, it is inferred that either the input profile is not an influential input or there are other influential inputs affecting the variations of these specific outputs.
- Based on the quantitative results obtained, the impact of the forecast uncertainty on the variability of the different KPIs (especially the indicator for the peak import power minimization which showed also occurrence of negative values) is quite crucial. This implies that reducing the uncertainty of this influential input helps in reducing the

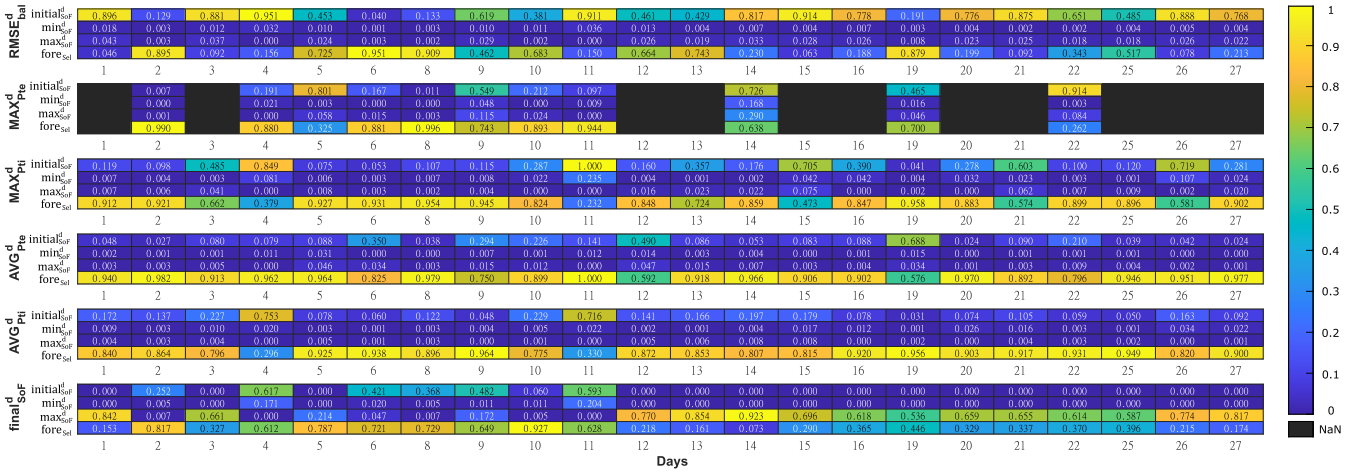

FIGURE 7. Total sensitivity indices for RBB. If the output variability is almost null, NaN value of the sensitivity indices are reported.

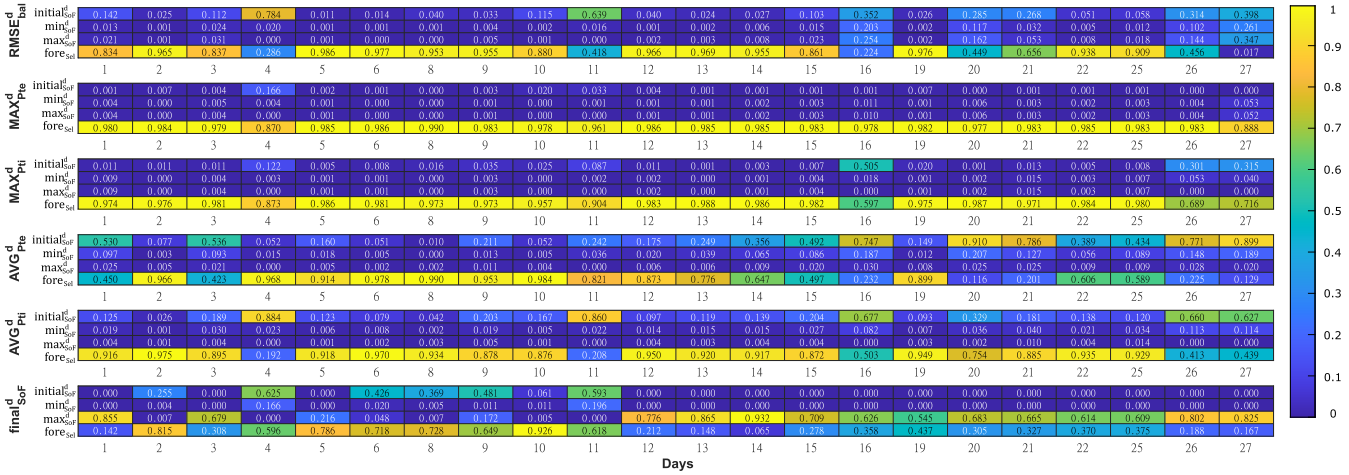

FIGURE 8. Total sensitivity indices for OPT.

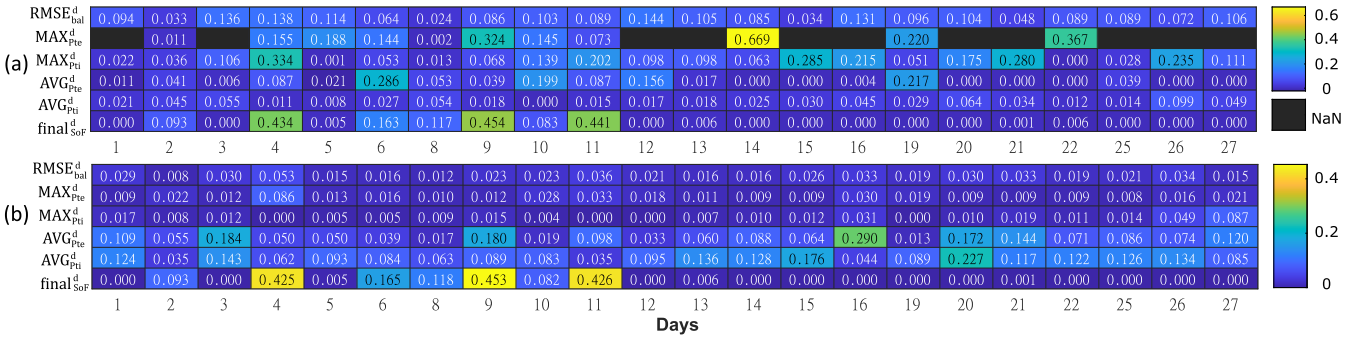

FIGURE 9. Total amount of interactions ($1 - \sum S_i$) in the model for (a) RBB and (b) OPT.

uncertainty in the KPI variations and can ultimately help significantly in avoiding the variations towards negative values. This reduces in the first place significantly the uncertainty in the expected outcome, paves the path for the EMS model revision in the second place and ultimately leads to the improvement in the EMS performance.

- Although observing that the SA ranking for different KPIs (for both RBB and OPT) guides the REC operator to prioritize the forecast uncertainty reduction as the first corrective action to reduce the uncertainty in the performance of the balancer for the majority of days, it has also been shown that, for certain days, flexibility-related parameters have a significant impact on the uncertainty of the balancer performance and should not be ignored.
- The variations in the flexibility-related input parameters, especially the initial state of flexibility, have bigger impact on the variability of the outputs of interest for

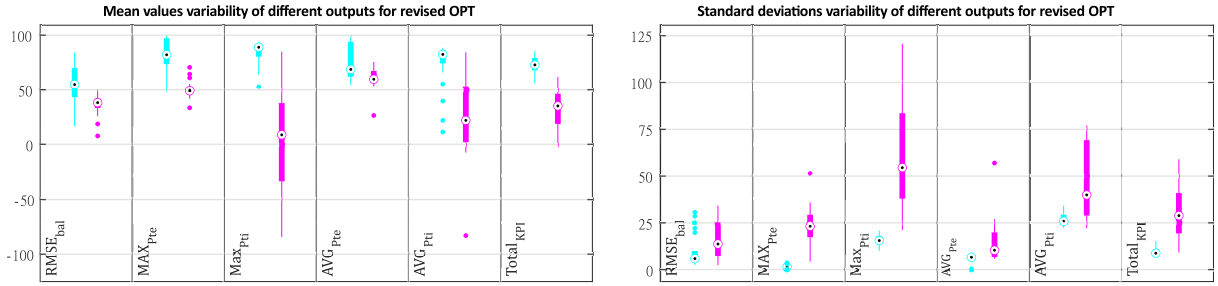

FIGURE 10. Mean and standard deviation variability over different days for the revised OPT. Cyan box plots represent the case when only measurement profile is used while magenta box plots represent the case when forecast and measurement profiles are used.

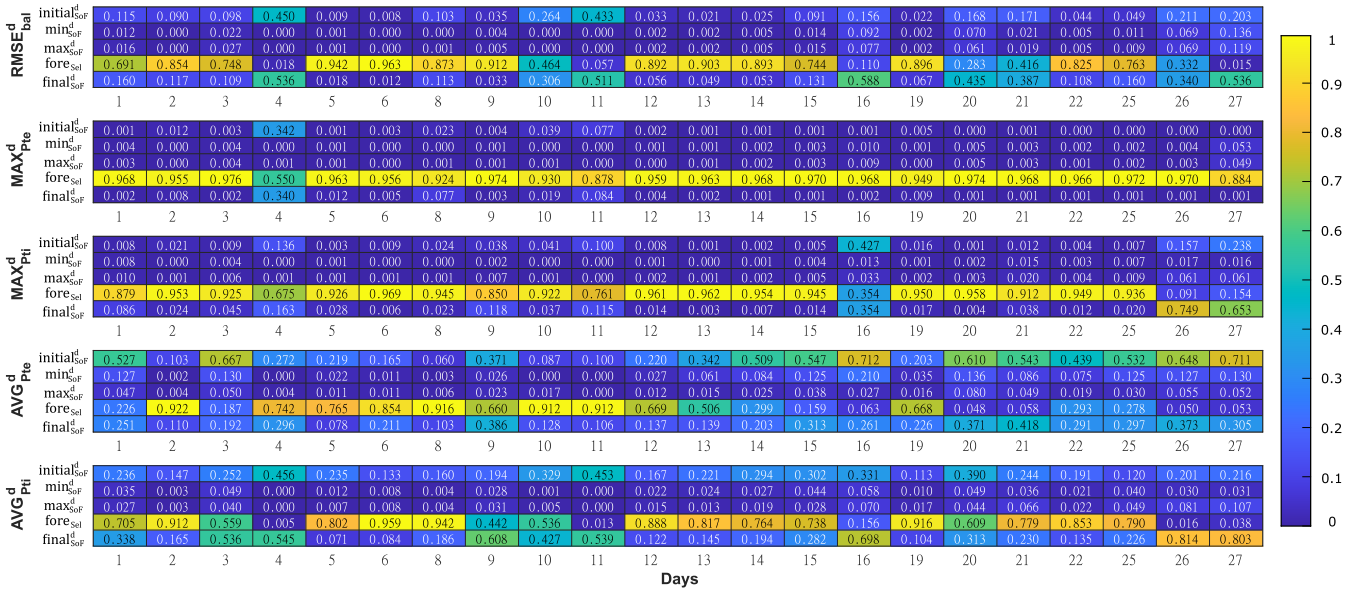

FIGURE 11. Total sensitivity indices for the revised OPT.

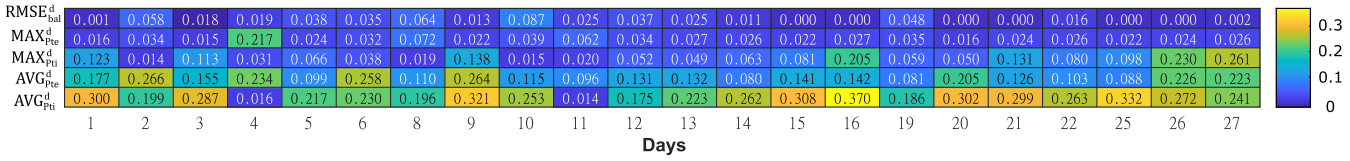

FIGURE 12. Total amount of interactions ($1 - \sum S_i$) in the model for the revised OPT.

RBB in comparison to OPT. Furthermore, the interactions among the different inputs affect the variability of outputs of interest for RBB more in comparison to OPT.

- Based on the GSA results, if the REC operator is willing to, there is a possibility of revising OPT accordingly (unlike RBB). In this work, such revision has been conducted for OPT by introducing $final^d_{SOF}$ as additional input and repeating the application of GSA on the revised model.
- For RBB and OPT and for almost all days, the two flexibility-related inputs of minimum and maximum state of flexibility are non-influential in the variations of KPIs and can be fixed at any value within their variation range. Furthermore, these inputs are not influential in the variations of the final state of flexibility as another output of interest, either.
- The revision of the OPT model with the inclusion of final state of flexibility as an additional input can increase the variability of the outputs, in this case KPIs, as they show sensitivity towards this newly introduced input variability. This is also accompanied by interaction with other inputs variability. The application of GSA for this revised model can allow the REC operator to identify the uncertainty and sensitivity associated with the different outputs of interest and take necessary actions to reduce uncertainty and/or improve the performance of the EMS. For this specific case, reducing the uncertainty in the variability of the new input parameter, i.e., $final^d_{SoF}$, according to an a-priori decision regarding the upcoming usage of the BESS by the REC operator, is of relevance. Furthermore, for the revised OPT, fixing the two flexibility-related inputs of minimum and maximum state of flexibility to any values within their ranges of

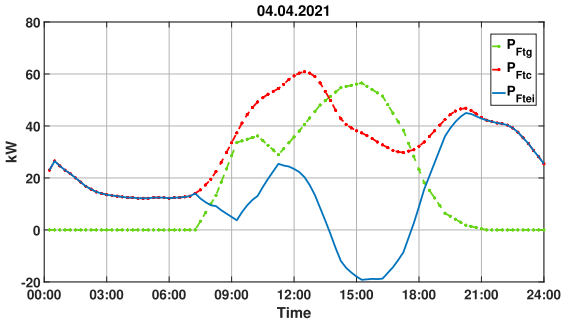

FIGURE 13. Generation, Consumption and net power forecast profiles.

variability can be done as they are not influential in the variability of outputs of interest for almost all days under study.

- The application of GSA provides detailed information about the importance of each input for each specific output of interest in a quantitative manner. Such information, in addition to supplementary data (e.g., meteorological data, provided that they will be available) are crucial for the REC operator to make clusters of operating periods for specific outputs of interest with the corresponding influential and non-influential input models, to reduce the model dimensionality, to possibly reduce uncertainty in the influential inputs and ultimately improve the model performance.

VI. RESULTS FOR THE FORECASTER

In the previous Section V-A, the results associated with the balancer, which is responsible for achieving the virtual islanding objective of the EMS, were presented. As one of the key findings, it was also highlighted that the uncertainty in the forecast can play an important role in the performance of the balancer in the scheduling mode. In light of this and knowing the EMS structure described in Section II and the operation boundaries associated with it (Subsection II-A), this section provides the simulation results for the forecaster module of the EMS.

A. FORECASTER PERFORMANCE

According to the mathematical formulation provided in (1) and based on the total generation (P_{Ftg}) and consumption (P_{Ftc}) forecast input profiles, the forecast profiles of the net active power exchange at the PCC (P_{Ftei}) could be calculated for the time horizon of this study. In Fig. 13, a typical example of such profiles is provided for the specific day of 04.04.2021.

As described in Subsection II-B1, the forecast profiles could be calibrated to generate more accurate profiles. Fig. 14 depicts the forecast profiles before and after the calibration (blue and red lines, respectively) along with the corresponding actual measurement values (orange line) for two different days. As observed in this figure, the calibration of the forecast profiles can lead to reasonable reductions in the forecast errors. With the forecast calibration mechanism, RMSE for the forecast of net active power exchange at the PCC is on average reduced around 12.5% for different days under study. Such reductions can even reach up to 33%. The reader can refer to Part 7 of the supplementary material to have a detailed look at corresponding reductions in the forecast errors.

In short and with respect to the forecaster performance results, it can be inferred that considering the low availability of historical data and other boundaries associated with the forecast module, the calibration can act as an intermediate measure to deliver an improved forecast. In Subsection V-A2, it has been also discussed how such an intermediate measure can restrain the negative impact on the performance of the balancer module and reduce the occurrence of negative KPIs. Provided that enough data (including the meteorological one) are at disposal of the REC operator, clusters of different days with respective calibrated scaling factors for each specific cluster can be made to improve the forecast uncertainty for different operational days.

B. RESULTS OF THE FORECASTER SENSITIVITY ANALYSIS

According to the methodology illustrated in Subsection III-B, before computing the sensitivity indices, uncertainty analysis is conducted to evaluate the uncertainty of the forecast prediction (i.e., $RMSE^d_{PFtei}$) given the uncertainty in the load and generation related inputs (i.e., $P^t_{F''_{tc}}$ and $P^t_{F''_{tg}}$ reported in Subsection IV-B).

An overview of the daily variability of the forecast errors in terms of $RMSE^d_{PFtei}$ is provided in Fig. 15 in the form of box plot representation, where mean, median, first and third quartiles of the forecast RMSE are shown. As it can be observed, the smallest average $RMSE^d_{PFtei}$ is reached on 04.04 and 11.04 with values of 12.4 kW and 18 kW, respectively, whereas in the rest of the month the average $RMSE^d_{PFtei}$ assume values around (or higher of) 40 KW. The highest average $RMSE^d_{PFtei}$ is observed on 06.04. Furthermore, the lowest and highest variability of the $RMSE^d_{PFtei}$ values are observed on 05.04 and 27.04, respectively. The reader can also refer to Part 8 of the supplementary material to have a look at the histogram example which can provide an insight about the data distribution associated with the uncertainty in the output of the forecaster module.

The box plot representation of Fig. 15 supplies information about the degree of confidence in the forecast estimate. The uncertainty of the forecast estimate (after being characterized and quantified) can be apportioned to the different sources of variability (i.e., the uncertainties of the load and generation). To this purpose, variance-based SA is performed to identify the most relevant inputs affecting the output of interest, i.e., the RMSE of the net active power exchange forecast ($RMSE^d_{PFtei}$). Analyzing the daily evolution of the sensitivity indices of P^d_{Ftg} and P^d_{Ftc} allows for assessing their relative importance on the $RMSE^d_{PFtei}$ over time. Fig. 16 reports the results for the total Sobol' indices, reflecting the importance of each input according to its overall effect. Null values of T_i signalize an inconsequential input, which could be hence fixed at any convenient value within its range of variation and removed from subsequent analyses. As observed in Fig. 16,

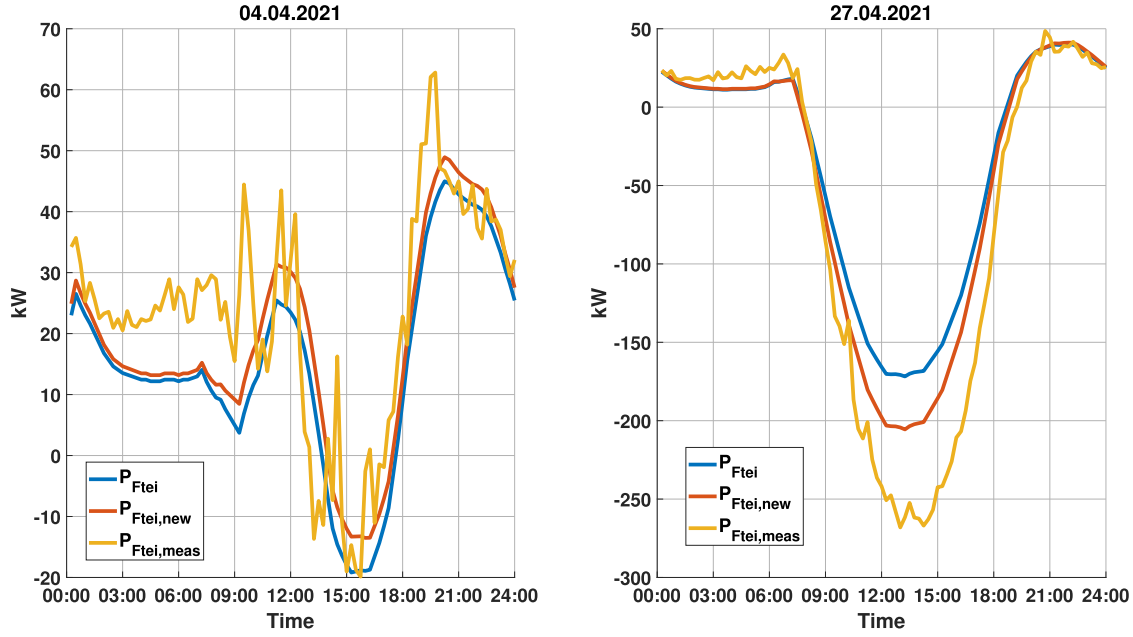

FIGURE 14. Forecast, calibrated forecast, and measurement profiles for 04.04.2021 and 27.04.2021.

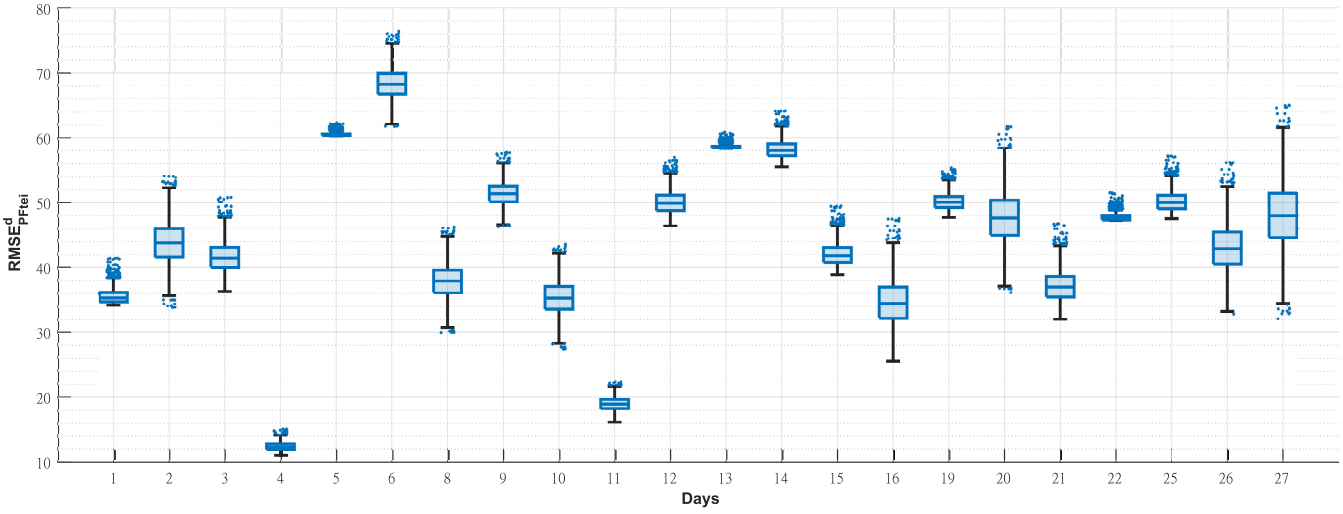

FIGURE 15. Box plot visualization for the variability of the forecaster error $RMSE^{d}_{PFtei}$.

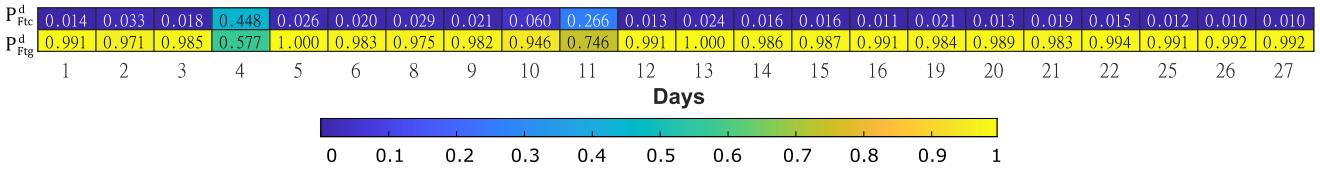

FIGURE 16. Total Sobol' indices for the forecaster.

P^{d}_{Ftg} is the most influential input for all days. Interestingly, on 04.04—for which the uncertainty is relatively low compared to other days, as reported in Fig. 15— P^{d}_{Ftg} and P^{d}_{Ftc} happen to have almost the same importance on the $RMSE^{d}_{PFtei}$ variability. It can hence be inferred that, on this specific day, the scaling of both total generation and consumption forecast profiles can affect the variance in the net active power forecast. On the other hand, on 27.04 (where the highest variability of $RMSE^{d}_{PFtei}$ was recorded as seen in Fig. 15), the consumption forecast has a negligible impact on the total forecast error ($T_i \approx 0$). In this case, the variability of the forecast error is almost entirely due to the variability of the scaling factor n^{d}_{tg}.

After performing the forecaster SA, from the above results it can be concluded that, in general, a resource investment for reducing the uncertainty in the total generation forecast of REC is inevitable. However, for the days characterized by a relatively limited amount of total renewable generation

considering the total installed capacity of 300 kWp and the corresponding net power exchange at the PCC (e.g., on 04.04 as shown on the left side of Fig. 14), the provided consumption and generation forecast profiles—respectively based on the SLP and the contractual agreement with the weather-data provider—lead to reasonably accurate forecast profiles with relatively low uncertainty, as seen in Fig. 15.

VII. CONCLUSION

This research work has presented the development of an EMS which consists of a balancer and a forecaster module and is in line with the virtual islanding scope of an REC field trial equipped with a BESS unit. Considering the availability of the field data and the associated boundary conditions, the RBB and OPT mechanisms of the developed balancer managed the REC in both measurement-and-steering and day-ahead scheduling modes based on (near) real-time measurements and forecast values, respectively. Given the unavoidable presence of specific sources of uncertainty potentially affecting the EMS performance, a thorough study of the EMS sensitivity behavior has also been conducted via GSA (by employing variance-based SA) with respect to multiple quantities specifically selected to encompass relevant aspects of the virtual islanding of the REC under study for its operator. In particular, different KPIs reflecting the performance of the developed balancer for minimizing the power exchange at the PCC and the final state of flexibility of the BESS have been selected as the outputs of interest. On the other hand and as inputs to investigate, the proposed multi-output GSA has considered not only flexibility-related parameters (such as the initial, minimum and maximum states of flexibility for the BESS), but also different levels of forecast accuracy that might affect the performance of the balancer. For the forecaster GSA, the total generation and consumption forecast profiles have been considered as inputs while the forecast error was selected as the output of interest. The thorough analysis using GSA has led to the identification of the most influential inputs affecting the desired performance of the EMS. Consequently and in this regard, EMS model inputs whose uncertainty is not crucial for certain outputs were also identified. In other terms, GSA helps in realizing the uncertainty of which model inputs could be neglected without affecting the output variability and provides solid basis for taking informed decisions e.g., in terms of model revisions and/or uncertainty reduction measures. For instance, for the OPT control mechanism of the developed EMS and for more than 95% of the days under study, the initial state of flexibility of the BESS, although being uncertain, had no impact on the variations of the KPI reflecting the minimization of maximum export power. In other words, the peak export reduction of the OPT mechanism is not typically (for 95% of the days) influenced by the initial state of the flexibility of the BESS. Hence, for such days, this might translate into the decision of the REC operator to allocate resources for decreasing the uncertainty of only the influential inputs to ultimately reduce the uncertainty of this KPI (or, in other words, enhance the EMS performance related to it). Furthermore, it was also discussed why it is necessary to comprehensively examine the EMS model including its revision(s) by GSA to capture both the positive and negative impacts on the EMS model uncertainty and performance. It was revealed for instance that the revision of the OPT model with the inclusion of final state of flexibility as an additional input requires additional attention as certain KPIs show sensitivity to this input while the minimum and maximum permissible states of flexibility of the BESS have a much less impact on those KPIs' variability after the model revision.

Moreover, it is of importance to highlight that, although in the first place one might assume that forecast uncertainty is the most influential input for the performance of the EMS, GSA results proved that flexibility-related inputs can also influence the uncertainty in the performance of the EMS: neglecting it would lead the operator to take incorrect decisions. Similarly, one might in the first place assume the ''obvious'' performance superiority of OPT over RBB mechanism for the developed EMS. This has indeed proved to be generally but not always true by looking at the values of the different KPIs. On the other hand, it was indeed shown though that such a judgmental superior performance is accompanied with almost the same amount of uncertainty for both of these mechanisms. It was only possible via GSA to quantitatively identify to which extent each of these mechanisms is sensitive towards the variations of the inputs of the balancer.

In view of the obtained results, it has emerged how the application of GSA is crucial to effectively support the uncertainty quantification of an EMS in order to ultimately provide the REC operator with a support tool for the decision making process in an uncertainty framework, e.g., to develop and revise EMS algorithms specifically designed for RECs. In this regard and by paving the path for future applications, this paper suggests the reusability of the proposed multi-output GSA for other similar EMS applications. For instance, a replicate of the developed EMS with the inclusion of other flexibility sources within the same REC under study or other RECs with different boundary conditions can be equally investigated following the workflow in this study. Furthermore and provided that sufficient data (including the meteorological one) are available, more advanced predicting algorithms (e.g., neural networks) can be used for reducing the uncertainty in the forecast values required for the scheduling mode of the developed EMS.

ACKNOWLEDGMENT

The authors would like to thank AVACON NETZ GmbH as part of the Consortium of the Platone Project for the collaborative support and providing the field trial data.

REFERENCES

[1] I. F. G. Reis, I. Gonçalves, M. A. R. Lopes, and C. H. Antunes, ''Assessing the influence of different goals in energy communities' self-sufficiency—An optimized multiagent approach,'' *Energies*, vol. 14, no. 4, p. 989, Feb. 2021.

[2] N. Hatziargyriou, *Microgrids: Architectures and Control*. Hoboken, NJ, USA: Wiley, 2013. [Online]. Available: https://onlinelibrary.wiley.com/doi/book/10.1002/9781118720677

[3] M. Hossain, H. Pota, W. Issa, and M. Hossain, "Overview of AC microgrid controls with inverter-interfaced generations," *Energies*, vol. 10, no. 9, p. 1300, Aug. 2017.

[4] F. Nejabatkhah and Y. W. Li, "Overview of power management strategies of hybrid AC/DC microgrid," *IEEE Trans. Power Electron.*, vol. 30, no. 12, pp. 7072–7089, Dec. 2015.

[5] I. Patrao, E. Figueres, G. Garcerá, and R. González-Medina, "Microgrid architectures for low voltage distributed generation," *Renew. Sustain. Energy Rev.*, vol. 43, pp. 415–424, Mar. 2015.

[6] B. P. Koirala, E. Koliou, J. Friege, R. A. Hakvoort, and P. M. Herder, "Energetic communities for community energy: A review of key issues and trends shaping integrated community energy systems," *Renew. Sustain. Energy Rev.*, vol. 56, pp. 722–744, Apr. 2016.

[7] Q. T. Tran, V. H. Nguyen, N. A. Luu, and E. Amicarelli, "Distributed energy resource management system," in *Local Electricity Markets*, T. Pinto, Z. Vale, and S. Widergren, Eds. New York, NY, USA: Academic, 2021, pp. 159–175.

[8] P. Balducci, K. Mongird, D. Wu, D. Wang, V. Fotedar, and R. Dahowski, "An evaluation of the economic and resilience benefits of a microgrid in Northampton, Massachusetts," *Energies*, vol. 13, no. 18, p. 4802, Sep. 2020.

[9] R. Faia, J. Soares, T. Pinto, F. Lezama, Z. Vale, and J. M. Corchado, "Optimal model for local energy community scheduling considering peer to peer electricity transactions," *IEEE Access*, vol. 9, pp. 12420–12430, 2021.

[10] M. Zulianello, V. Angelucci, and D. Moneta, "Energy community and collective self consumption in Italy," in *Proc. 55th Int. Universities Power Eng. Conf. (UPEC)*, Sep. 2020, pp. 1–5.

[11] C. Gallego-Castillo, M. Heleno, and M. Victoria, "Self-consumption for energy communities in Spain: A regional analysis under the new legal framework," *Energy Policy*, vol. 150, Mar. 2021, Art. no. 112144.

[12] F. Katiraei and J. Aguero, "Solar PV integration challenges," *IEEE Power Energy Mag.*, vol. 9, no. 3, pp. 62–71, May 2011.

[13] A. Povlsen, "Impacts of power penetration from photovoltaic power systems in distribution networks," International Energy Agency (IEA), Paris, France, Tech. Rep., IEA PVPS T5-10, 2002.

[14] B. Ansari, D. Shi, R. Sharma, and M. G. Simoes, "Economic analysis, optimal sizing and management of energy storage for PV grid integration," in *Proc. IEEE/PES Transmiss. Distrib. Conf. Expo.*, May 2016, pp. 1–5.

[15] *Standard for Interconnecting Distributed Resources With Electric Power Systems*, IEEE Standard 1547, 2014.

[16] R. Mahmud, A. Hoke, and D. Narang, "Validating the test procedures described in UL 1741 SA and IEEE P1547.1," in *Proc. IEEE 7th World Conf. Photovoltaic Energy Convers.*, Jun. 2018, pp. 1445–1450.

[17] X. Liu, A. Aichhorn, L. Liu, and H. Li, "Coordinated control of distributed energy storage system with tap changer transformers for voltage rise mitigation under high photovoltaic penetration," *IEEE Trans. Smart Grid.*, vol. 3, no. 2, pp. 897–906, Jun. 2012.

[18] Y. Yang, H. Li, A. Aichhorn, J. Zheng, and M. Greenleaf, "Sizing strategy of distributed battery storage system with high penetration of photovoltaic for voltage regulation and peak load shaving," *IEEE Trans. Smart Grid*, vol. 5, no. 2, pp. 982–991, Mar. 2014.

[19] D. Shi and R. K. Sharma, "Adaptive control of energy storage for voltage regulation in distribution system," in *Proc. IEEE Int. Conf. Smart Energy Grid Eng. (SEGE)*, Aug. 2013, pp. 1–7.

[20] F. Lezama, J. Soares, P. Hernandez-Leal, M. Kaisers, T. Pinto, and Z. Vale, "Local energy markets: Paving the path toward fully transactive energy systems," *IEEE Trans. Power Syst.*, vol. 34, no. 5, pp. 4081–4088, Sep. 2019.

[21] J. K. Kok, C. J. Warmer, and I. G. Kamphuis, "PowerMatcher: Multiagent control in the electricity infrastructure," in *Proc. 4th Int. Joint Conf. Auto. Agents Multiagent Syst.*, Jul. 2005, pp. 75–82.

[22] J. M. Raya-Armenta, N. Bazmohammadi, J. G. Avina-Cervantes, D. Sáez, J. C. Vasquez, and J. M. Guerrero, "Energy management system optimization in islanded microgrids: An overview and future trends," *Renew. Sustain. Energy Rev.*, vol. 149, Oct. 2021, Art. no. 111327.

[23] G. S. Thirunavukkarasu, M. Seyedmahmoudian, E. Jamei, B. Horan, S. Mekhilef, and A. Stojcevski, "Role of optimization techniques in microgrid energy management systems—A review," *Energy Strategy Rev.*, vol. 43, Sep. 2022, Art. no. 100899.

[24] M. F. Zia, E. Elbouchikhi, and M. Benbouzid, "Microgrids energy management systems: A critical review on methods, solutions, and prospects," *Appl. Energy*, vol. 222, pp. 1033–1055, Jul. 2018.

[25] A. Elmouatamid, R. Ouladsine, M. Bakhouya, N. E. Kamoun, M. Khaidar, and K. Zine-Dine, "Review of control and energy management approaches in micro-grid systems," *Energies*, vol. 14, no. 1, p. 168, Dec. 2020.

[26] M. Warneryd, M. Håkansson, and K. Karltorp, "Unpacking the complexity of community microgrids: A review of institutions' roles for development of microgrids," *Renew. Sustain. Energy Rev.*, vol. 121, Apr. 2020, Art. no. 109690.

[27] Y. Zahraoui, I. Alhamrouni, S. Mekhilef, M. R. Basir Khan, M. Seyedmahmoudian, A. Stojcevski, and B. Horan, "Energy management system in microgrids: A comprehensive review," *Sustainability*, vol. 13, no. 19, p. 10492, Sep. 2021.

[28] M. Li, L. Wang, Y. Wang, and Z. Chen, "Sizing optimization and energy management strategy for hybrid energy storage system using multiobjective optimization and random forests," *IEEE Trans. Power Electron.*, vol. 36, no. 10, pp. 11421–11430, Oct. 2021.

[29] A. Giordano, C. Mastroianni, L. Scarcello, and G. Spezzano, "An optimization model for efficient energy exchange in energy communities," in *Proc. 5th Int. Conf. Fog Mobile Edge Comput. (FMEC)*, Apr. 2020, pp. 319–324.

[30] D. Mildt, M. Cupelli, and A. Monti, "Objective trade-off in MPC based energy management for microgrids," in *Proc. IEEE PES GTD Grand Int. Conf. Expo. Asia (GTD Asia)*, Mar. 2019, pp. 280–285.

[31] K. M. M. Huq, M. E. Baran, S. Lukic, and O. E. Nare, "An energy management system for a community energy storage system," in *Proc. IEEE Energy Convers. Congr. Expo. (ECCE)*, Sep. 2012, pp. 2759–2763.

[32] M. Castillo-Cagigal, E. Caamaño-Martín, E. Matallanas, D. Masa-Bote, A. Gutiérrez, F. Monasterio-Huelin, and J. Jiménez-Leube, "PV self-consumption optimization with storage and active DSM for the residential sector," *Sol. Energy*, vol. 85, no. 9, pp. 2338–2348, Sep. 2011.

[33] L. Fialho, T. Fartaria, L. Narvarte, and M. Collares Pereira, "Implementation and validation of a self-consumption maximization energy management strategy in a vanadium redox flow BIPV demonstrator," *Energies*, vol. 9, no. 7, p. 496, Jun. 2016.

[34] M. Nasr, A. Rabiee, and I. Kamwa, "MPC and robustness optimisation-based EMS for microgrids with high penetration of intermittent renewable energy," *IET Gener., Transmiss. Distrib.*, vol. 14, no. 22, pp. 5239–5248, Nov. 2020.

[35] E. Craparo, M. Karatas, and D. I. Singham, "A robust optimization approach to hybrid microgrid operation using ensemble weather forecasts," *Appl. Energy*, vol. 201, pp. 135–147, Sep. 2017.

[36] L. Wang, Q. Li, R. Ding, M. Sun, and G. Wang, "Integrated scheduling of energy supply and demand in microgrids under uncertainty: A robust multi-objective optimization approach," *Energy*, vol. 130, pp. 1–14, Jul. 2017.

[37] R. A. Gupta and N. K. Gupta, "A robust optimization based approach for microgrid operation in deregulated environment," *Energy Convers. Manage.*, vol. 93, pp. 121–131, Mar. 2015.

[38] L. Wen, K. Zhou, S. Yang, and X. Lu, "Optimal load dispatch of community microgrid with deep learning based solar power and load forecasting," *Energy*, vol. 171, pp. 1053–1065, Mar. 2019.

[39] M. Ruiz-Cortes, E. Gonzalez-Romera, R. A. Lopes, E. Romero-Cadaval, J. Martins, M. I. Milanas-Montero, and F. Barreto-Gonzalez, "Improved forecasting-based battery energy management strategy for prosumer systems," in *Proc. 44th Annu. Conf. IEEE Ind. Electron. Soc.*, Oct. 2018, pp. 6077–6082.

[40] M. Ginocchi, F. Ponci, and A. Monti, "Sensitivity analysis and power systems: Can we bridge the gap? A review and a guide to getting started," *Energies*, vol. 14, no. 24, p. 8274, Dec. 2021.

[41] Platone. *PLATform for Operation of Distribution Networks—German Demo Deliverables (D5.x)*. Accessed: Jan. 10, 2023. [Online]. Available: https://platone-h2020.eu/Project/Deliverables

[42] A. Shirsat and W. Tang, "Sensitivity analysis of time-of-use rates on operations of home energy management systems," in *Proc. IEEE Power & Energy Soc. Gen. Meeting (PESGM)*, Aug. 2020, pp. 1–5.

[43] M. Tasdighi, H. Ghasemi, and A. Rahimi-Kian, "Residential microgrid scheduling based on smart meters data and temperature dependent thermal load modeling," *IEEE Trans. Smart Grid*, vol. 5, no. 1, pp. 349–357, Jan. 2014.

[44] X. Xu, Z. Yan, M. Shahidehpour, S. Chen, H. Wang, Z. Li, and Q. Zhou, "Maximum loadability of islanded microgrids with renewable energy generation," *IEEE Trans. Smart Grid*, vol. 10, no. 5, pp. 4696–4705, Sep. 2019.
[45] BDEW. *Anwendung der Repräsentativen VDEWLastprofile Step by Step*. Accessed: Jan. 10, 2023. [Online]. Available: https://www.bdew.de/energie/standardlastprofile-strom/
[46] Meteoblue. *Meteoblue APIs, Weather Models, Datasets, Services and Variables*. Accessed: Jan. 10, 2023. [Online]. Available: https://docs.meteoblue.com/en
[47] A. Saltelli, M. Ratto, T. Andres, F. Campolongo, J. Cariboni, D. Gatelli, M. Saisana, and S. Tarantola, *Global Sensitivity Analysis. The Primer*. Chichester, U.K.: Wiley, 2008.
[48] I. M. Sobol, "Sensitivity analysis for non-linear mathematical models," *Math. Modell. Comput. Exp.*, vol. 1, no. 4, pp. 407–414, 1993.
[49] T. Homma and A. Saltelli, "Importance measures in global sensitivity analysis of nonlinear models," *Rel. Eng. Syst. Saf.*, vol. 52, no. 1, pp. 1–17, 1996.
[50] H. Niederreiter, *Random Number Generation and Quasi-Monte Carlo Methods*. Philadelphia, PA, USA: SIAM, 1992.
[51] I. M. Sobol and S. S. Kucherenko, "On global sensitivity analysis of quasi-Monte Carlo algorithms," *Monte Carlo Methods Appl.*, vol. 11, no. 1, pp. 83–92, Mar. 2005.
[52] Y. Wang, N. Zhang, Q. Chen, D. S. Kirschen, P. Li, and Q. Xia, "Data-driven probabilistic net load forecasting with high penetration of behind-the-meter PV," *IEEE Trans. Power Syst.*, vol. 33, no. 3, pp. 3255–3264, May 2018.
[53] S. Govender and K. A. Folly, "Short-term load forecasting using artificial neural networks and multiple linear regression," in *Proc. IEEE PES/IAS PowerAfrica*, Aug. 2019, pp. 273–278.
[54] A. Wächter and L. T. Biegler, "On the implementation of an interior-point filter line-search algorithm for large-scale nonlinear programming," *Math. Program.*, vol. 106, no. 1, pp. 25–57, May 2006.
[55] W. E. Hart, J.-P. Watson, and D. L. Woodruff, "Pyomo: Modeling and solving mathematical programs in Python," *Math. Program. Comput.*, vol. 3, no. 3, p. 219, 2011.

AMIR AHMADIFAR (Member, IEEE) received the M.Sc. degree in electrical engineering, information technology and computer engineering from RWTH Aachen University, Aachen, Germany, in 2017. He is currently a Research Associate with the E.ON Energy Research Center, Institute for Automation of Complex Power Systems, RWTH Aachen University. His current research interests include power system modeling, analysis, and control, smart management of active distribution grids, and renewable energies integration in smart grids with high levels of electric mobility.

MIRKO GINOCCHI received the M.Sc. degree in sciences and technology for environment and landscape from the University of Milano-Bicocca, Milan, Italy, in 2014. He joined the Sensitivity Analysis of Model Output Group of the Competence Centre on Modeling, European Commission Joint Research Centre, Ispra, Italy, in 2016. He joined the Institute for Automation of Complex Power Systems, E.ON Energy Research Center, RWTH Aachen University, Aachen, Germany, in 2018. His current research interests include uncertainty and sensitivity analysis for power system applications.

MEGHA SHYAM GOLLA received the M.Sc. degree in management and engineering with electrical power systems from RWTH Aachen University, Germany, in 2021. He was a Student Research Assistant at the E.ON Energy Research Center, Institute for Automation of Complex Power Systems, RWTH Aachen University, Germany, and wrote the master thesis in the area of load forecasting for distribution networks. He is currently a Development Engineer with Venios GmbH, Frankfurt, Germany. His current interest includes developing various solutions for grid digitalization.

FERDINANDA PONCI (Senior Member, IEEE) received the Ph.D. degree in electrical engineering from the Politecnico di Milano, Italy, in 2002. She joined as an Assistant Professor at the Department of Electrical Engineering, University of South Carolina, Columbia, SC, USA, in 2003, and was tenured and promoted, in 2008. In 2009, she joined the E.ON Research Center, Institute for Automation of Complex Power Systems, RWTH Aachen University, Aachen, Germany, where she is currently a Professor of monitoring and distributed control for power systems. Her research interests include advanced measurement, monitoring, and automation of active distribution systems. She is an Elected Member of the Administration Committee of the IEEE Instrumentation and Measurement Society and the Liaison with IEEE Women in Engineering.

ANTONELLO MONTI (Senior Member, IEEE) received the M.Sc. (summa cum laude) and Ph.D. degrees in electrical engineering from the Politecnico di Milano, Italy, in 1989 and 1994, respectively. He started his career at Ansaldo Industria and then moved to the Politecnico di Milano as an Assistant Professor, in 1995. In 2000, he joined as an Associate Professor at the Department of Electrical Engineering, University of South Carolina, USA, and then a Full Professor. Since 2008, he has been the Director of the E.ON Energy Research Center, Institute for Automation of Complex Power System, RWTH Aachen University. Since 2019, he has been holding a double appointment with the Fraunhofer FIT, where he is developing the new Center for Digital Energy, Aachen. He is the author or coauthor of more than 400 peer-reviewed papers published in international journals and in the proceedings of international conferences. He was a recipient of the 2017 IEEE Innovation in Societal Infrastructure Award. He is an Associate Editor of the IEEE Systems Journal, an Associate Editor of *IEEE Electrification Magazine*, a member of the Editorial Board of the *SEGAN* (Elsevier) journal, and a member of the Founding Board of the *Energy Informatics* (Springer) journal.